

**Effects of Pt loading onto SnO₂ electrodes on CO-sensing properties
and mechanism of potentiometric gas sensors
utilizing an anion-conducting polymer electrolyte**

Takeo Hyodo*, Toshiyuki Goto, Mari Takamori, Taro Ueda, and Yasuhiro Shimizu

*Graduate School of Engineering, Nagasaki University
1-14 Bunkyo-machi, Nagasaki 852-8521, Japan*

*Corresponding author:

Takeo Hyodo, Dr.

Graduate School of Engineering, Nagasaki University

1-14 Bunkyo-machi, Nagasaki 852-8521, Japan

Tel: +81-95-819-2644

Fax: +81-95-819-2643

E-mail: hyodo@nagasaki-u.ac.jp

ABSTRACT

Gas-sensing properties of electrochemical CO sensors utilizing Pt-loaded SnO₂ electrodes and an anion-conducting polymer electrolyte have been investigated mainly at 30°C in wet synthetic air (57%RH), and the effects of the Pt loading onto SnO₂ on the CO-sensing properties and their CO-sensing mechanism have been discussed in this paper. The amount of Pt loaded onto SnO₂ (0.5–5.0 wt%) and the subsequent heat-treatment at 500°C in air were effective in enhancing the CO responses and the CO selectivity against H₂. The sensing-electrode potential was governed by mixed potential resulting from electrochemical CO (or H₂) oxidation and O₂ reduction, and all the results obtained indicated that the oxidation rate of CO molecules was electrochemically quite faster than that of H₂ molecules on the mono-dispersive and oxidized Pt species as an active site, which were doped at the surface SnO₂ lattice. On the other hand, the heat treatment at 250°C in H₂ after the Pt loading reduced the surface of Pt-loaded SnO₂ and drastically enhanced both CO and H₂ responses and thus decreased the CO selectivity against H₂. This effect arose probably from the reduced Pt species with metallic surface, which were quite active against both CO and H₂ anodic reactions.

KEYWORDS: carbon monoxide, gas sensor, tin dioxide, platinum, anion-conducting polymer

1. INTRODUCTION

Some kinds of electrochemical gas sensors operable at room temperature (RT) have been utilized to various application fields such as gas-leak detectors, alcohol and breath-odor checkers, oxygen and toxic-gas (e.g., hydrogen sulfide, ammonia, CO) monitors, and so on. Most of these sensors have generally used highly ionic-conductive liquid electrolytes such as sulfonic acid aqueous solutions [1–4], but they have some problems on the operation stability due to vaporization of the liquid electrolytes and a decrease in the reaction sites (i.e., three-phase boundaries) in the electrodes during long-term use. Therefore, some inorganic solid electrolytes such as lanthanum fluoride [5], antimonite acid [6], and ion liquids [7, 8] have been ever studied as an alternative electrolyte for the gas sensors operable at RT. Proton-conducting polymers, such as Nafion[®], are the most attractive as an electrolyte for their gas sensors, because they have large proton conductivity and relatively excellent long-term stability, and thus they have already been utilized as an excellent electrolyte for polymer electrolyte fuel cells (PEFC) [9–13]. Many researchers have also studied electrochemical gas sensors using the proton-conducting polymer electrolyte, and some types of these electrochemical CO sensors are presently commercialized all over the world [14]. Anion-conducting polymers (ACP) with large hydroxide ion (OH⁻) conductivity and improved long-term stability have been also gained attention as an electrolyte for electrochemical power devices such as PEFC, because it was operated under large current density as well as high power density with relatively-low overpotential [15–19]. Thus, the ACP has been promising also for gas-sensing applications. On the other hand, carbon-based materials loaded with a large amount of noble-metal nanoparticles (mainly, Pt or Pd) or just noble metals have been generally used as a sensing-electrode material, because of the quite large electrocatalytic activity and chemical stability of the noble-metals and the large specific surface area, relatively large chemical stability, and the low cost of the carbon-based materials [1–3, 9–14]. The amount of the noble metals loaded onto the carbon-based materials are quite large (generally, several tens %). However, these noble metals were well known to be electrochemically quite active against various redox reactions, and thus the sensors employing the carbon electrodes loaded with noble metals generally show large responses to various gases, which means that their gas selectivity was relatively low [20, 21]. We have recently focused on various kinds of metal oxides as a CO-sensing electrode material for electrochemical gas sensors using the ACP electrolyte [22, 23], and we have demonstrated that SnO₂ loaded with 2.0 wt% Pt nanoparticles is one of promising candidates for the CO-sensing electrode material among various combinations between metal oxides and loaded noble metals [24]. However, we did not understand the reasons why the loading of Pt nanoparticles effectively improved the CO-sensing properties of the sensors using the SnO₂ sensing electrode. In this study, therefore, the various amounts of Pt were loaded onto the SnO₂, and the morphology and chemical states of the Pt-loaded SnO₂

(especially, Pt) were controlled by annealing under different conditions. The CO-sensing properties (CO selectivity against H₂ as well as CO response (sensitivity)) of the sensors using the obtained *n* wt% Pt-loaded SnO₂ electrodes (*n*: 0.1–10) were measured, and the effects of their morphology and chemical states on the CO-sensing properties and mechanism were discussed in this paper.

2. EXPERIMENTAL

A SnO₂ powder was prepared according to the following procedure. The pH of 0.17 M SnCl₄ aqueous solution was adjusted to 2.0 by the addition of a NH₃ aqueous solution. The obtained precipitate was centrifuged and washed with pure water repeatedly, and then dried at 100°C. Then, a pristine SnO₂ powder was obtained after the calcination of the resultant powder at 500°C for 3 h in air. A Pt-loaded SnO₂ powder was prepared by general impregnation technique. After an appropriate amount of the SnO₂ powder was added to a 1 mM PtCl₄ aqueous solution, the obtained solution containing the SnO₂ powder was ultrasonicated at RT for 10 min and then it was evaporated to dryness. Then, the resultant solid was heat-treated in air at 500°C for 1 h or in H₂ at 250°C for 1 h. The heat-treatment conditions were decided on the basis of our previous findings [23–25] and preliminarily experimental results. The obtained *n* wt% Pt-loaded SnO₂ powder heat-treated in air at 500°C for 1 h or in H₂ at 250°C for 1 h (*n*: 0.1, 0.5, 2.0, 5.0, 7.0, 10) was denoted as *n*Pt/SnO₂(500air) and *n*Pt/SnO₂(250H₂), respectively. Crystal phases of all powders prepared were characterized by X-ray diffraction analysis (XRD; Rigaku Corp., RINT2200) using Cu K α radiation (40 kV, 36 mA), and their crystallite sizes (CS) were calculated by utilizing the Scherrer equation (shaper factor: 0.9). Pore size distributions and specific surface areas (SSA) of all the powders were measured by general Barrett–Joyner–Halenda (BJH) and Brunauer–Emmett–Teller (BET) methods using N₂ adsorption-desorption isotherms (Micromeritics Inst. Corp., TriStar 3000), respectively. Chemical states of elements on the surface of representative powders were characterized by X-ray photoelectron spectroscopy using Al K α radiation (XPS, Kratos, ACIS-TLATRA DLD), and the binding energy was calibrated using the C 1s level (285.0 eV) from usual contamination. In some cases, sputtering with 5 keV Ar⁺ was performed to clean the surface of the powders.

A schematic drawing of a sensor element is shown in Fig. S1(a). The obtained powder was mixed with an ACP solution (AS-4, Tokuyama Corp.), which is *iso*-propanol containing a 5 wt% hydrocarbon-type ionic polymer with quaternary ammonium salts (the powder : ACP = 95 : 5 in weight). The paste obtained was applied on the surface of both sides of an ACP membrane (A201, Tokuyama Corp., a polyolefin polymer film which consists of hydrocarbon main chain and quaternary ammonium salts, thickness: ca. 30 μ m) as sensing and counter electrodes by blade coating, and then it was dried at ca. 50°C for

30 min. The sensor elements were denoted as EC(SnO₂), EC(*n*Pt/SnO₂(500air)) or EC(*n*Pt/SnO₂(250H₂)). Here, EC stands for electrochemical cell. A schematic drawing of a gas-sensing measurement system is shown in Fig. S1(b). The sensor element was sandwiched with Au meshes (Nilaco, 100 mesh) as a current collector and was set up in a gas-sensing measurement system with two electrode compartments. Electromotive force (*E*) of all sensors to CO or H₂ (10–3000 ppm) balanced with wet synthetic air (O₂: 20%, N₂: 80%, relative humidity: 57%RH at 30°C), which was flowed over the sensing electrode, was measured at 30°C by using a digital electrometer (ADCMT, 8240), while the wet synthetic air was flowed over the counter electrode. The magnitude of response was defined as a change in *E* value induced by a sample gas (ΔE_{SG} , SG (sample gas): CO or H₂). CO selectivity against H₂ was defined as a ratio of CO response to H₂ response ($\Delta E_{CO}/\Delta E_{H_2}(c)$, *c*: concentration of CO and H₂).

3. RESULTS AND DISCUSSION

3.1 CO-sensing properties of EC(2Pt/SnO₂(500air)) and EC(2Pt/SnO₂(250H₂)) sensors

The EC(SnO₂) sensor, which used pristine SnO₂ as a sensing-electrode material, showed only small responses to both 500 ppm CO and 500 ppm H₂ ($\Delta E_{CO}(500)$: ca. 2.7 mV, $\Delta E_{H_2}(500)$: ca. 1.0 mV) in the negative *E* direction, and the *E* value was quite unstable, as shown in our previous paper [23]. However, the loading of 2 wt% Pt onto SnO₂ as a sensing-electrode material and subsequent heat treatment (in air at 500°C for 1 h, or in H₂ at 250°C for 1 h) drastically improved the signal/noise (S/N) ratio as well as the magnitude of both the CO and H₂ responses of the EC(SnO₂) sensor. Figure 1 shows response transients of the EC(2Pt/SnO₂(500air)) and EC(2Pt/SnO₂(250H₂)) sensors to 10–3000 ppm CO and H₂ balanced with wet synthetic air at 30°C (57% relative humidity (RH)) and Fig. 2 shows concentration dependences of CO and H₂ responses of the EC(2Pt/SnO₂(500air)) and EC(2Pt/SnO₂(250H₂)) sensors, together with their CO and H₂ sensitivities. Table 1 shows their 90% response and 70% recovery times to 10 ppm and 3000 ppm CO and H₂. Please note that all symbols used in this paper are listed in Appendix. Among these data, only their response transients to 500 ppm CO and H₂ and the magnitude of their responses have simply been discussed in our previous paper, in comparison with those of various EC(EM) sensor (EM (electrode material annealed in air at 500°C or in H₂ at 250°C): 2 wt% N-loaded MO, N (noble metal): Ag, Au, Pd, Ir, Ru, Rh; MO (metal oxide): Bi₂O₃, CeO₂, In₂O₃, V₂O₅) [25]. Both the EC(2Pt/SnO₂(500air)) and EC(2Pt/SnO₂(250H₂)) sensors showed quite large CO responses in comparison with that of the EC(SnO₂) sensor, and the magnitude of their CO responses was proportional to the logarithm of CO concentration. The CO response of the EC(2Pt/SnO₂(500air)) sensor was smaller than that of the EC(2Pt/SnO₂(250H₂)) sensor, especially in the higher CO concentration range (e.g.,

$\Delta E_{CO}(500)$: ca. 102 mV for the EC(2Pt/SnO₂(500air)) sensor and ca. 221 mV for the EC(2Pt/SnO₂(250H₂)) sensor). However, the CO response of the EC(2Pt/SnO₂(500air)) sensor was comparable to that of the EC(2Pt/SnO₂(250H₂)) sensor in the lower CO concentration range, and thus the CO sensitivity of the EC(2Pt/SnO₂(500air)) sensor (ca. 53.5 mV/decade) was much smaller than that of the EC(2Pt/SnO₂(250H₂)) sensor (ca. 121 mV/decade). These sensors showed much faster response and recovery speeds than those of the EC(SnO₂) sensor [23]. The response and recovery times of both the sensors obviously decreased with an increase in the CO concentration, as shown in Table 1. The loading of 2 wt% Pt onto SnO₂ improved also the H₂ responses of both the sensors, but the effectiveness was largely dependent on the subsequent heat-treatment conditions. Namely, the EC(2Pt/SnO₂(250H₂)) sensor showed the quite large response to H₂ (e.g., $\Delta E_{H_2}(500)$: ca. 117 mV) and the large H₂ sensitivity (ca. 86.9 mV/decade), and thus the CO selectivity of the sensor against H₂ ($\Delta E_{CO}/\Delta E_{H_2}(500)$: ca. 1.9) was smaller than that of the EC(SnO₂) sensor ($\Delta E_{CO}/\Delta E_{H_2}(500)$: ca. 2.7 [23]). On the other hand, the H₂ response of the EC(2Pt/SnO₂(500air)) sensor (e.g., $\Delta E_{H_2}(500)$: ca. 12.3 mV) was much smaller than that of the EC(2Pt/SnO₂(250H₂)) sensor, and its H₂ sensitivity was also quite small (ca. 14.5 mV/decade). Therefore, the EC(2Pt/SnO₂(500air)) sensor showed much larger CO selectivity of the sensor against H₂ ($\Delta E_{CO}/\Delta E_{H_2}(500)$: ca. 8.3) than the EC(2Pt/SnO₂(250H₂)) sensor. The response and recovery times of both the sensors to H₂ also decreased with an increase in the H₂ concentration, and the response and recovery speeds of the EC(2Pt/SnO₂(250H₂)) sensor were much faster than those of the EC(2Pt/SnO₂(500air)) sensor. By the way, the heat treatment of Au-loaded SnO₂ gave an extremely different effects on the CO-sensing properties from that of the Pt-loaded SnO₂, as shown in our previous paper [23]. Namely, the heat treatment of the Au-loaded SnO₂ in air at elevated temperatures increased the H₂ response as well as the CO response (CO response > H₂ response), while the heat treatment of the Au-loaded SnO₂ in H₂ at elevated temperatures increased only the CO response and thus increased the CO selectivity against H₂. These differences indicate that the Pt species on the SnO₂ surface fulfilled a completely different electrocatalytic role on the CO and H₂ responses from the Au species on the SnO₂ surface.

Various physical properties of 2Pt/SnO₂(500air) and 2Pt/SnO₂(250H₂) powders were investigated to clarify the large differences in CO-sensing properties between the EC(2Pt/SnO₂(500air)) and EC(2Pt/SnO₂(250H₂)) sensors. Figure S2 shows X-ray diffraction (XRD) spectra of pristine SnO₂, 2Pt/SnO₂(500air), and 2Pt/SnO₂(250H₂) powders, together with their SnO₂ crystallite size (CS) which was calculated with the (110) peak by using the Scherrer equation. In addition, N₂ adsorption-desorption isotherms and pore size distributions of these powders are shown in Fig. S3, together with their specific

surface areas (SSA). The XRD spectrum of the pristine SnO₂ powder was attributed to a single phase of SnO₂ cassiterite (tetragonal, JCPDS No. 01-075-2893), and the CS was ca. 7.9 nm. The CS values of the 2Pt/SnO₂(500air) and 2Pt/SnO₂(250H₂) powders were ca. 6.8 and ca. 7.3 nm, respectively, which were slightly smaller than that of the pristine SnO₂ powder. The XRD peak of any Pt components was not confirmed for the 2Pt/SnO₂(500air) and 2Pt/SnO₂(250H₂) powders. On the other hand, the N₂ adsorption-desorption isotherms of the pristine SnO₂ powder, which had relatively large SSA (ca. 48.2 m² g⁻¹), belong to "Type IV" according to the BET classification [26]. The hysteresis behavior is associated with capillary condensation and evaporation of N₂, based on their well-developed ink-bottle mesopores. The loading of Pt onto SnO₂ and subsequent heat-treatment hardly influenced on the SSA value, but slightly reduced the size of mesopores. From these results, it is confirmed that the differences in CO-sensing properties between of EC(2Pt/SnO₂(500air)) and the EC(2Pt/SnO₂(250H₂)) sensors cannot be ascribed to the change in physical properties of electrode materials.

On the other hand, the difference in the heat-treatment condition had a quite large influence on the chemical state on the surface. Figure 3 shows X-ray photoelectron spectroscopy (XPS) spectra of Pt 4f of 2Pt/SnO₂(500air) and 2Pt/SnO₂(250H₂) powders. The large amount of Pt was oxidized (Pt⁴⁺: 40.6%, Pt²⁺: 46.6%, Pt⁰ metal: 12.8%) at the surface of the 2Pt/SnO₂(500air) powder, and the Ar etching easily reduced the polyvalent Pt components (Pt⁴⁺ and Pt²⁺) to produce Pt⁰ metals. In contrast, Pt atoms at the surface of the 2Pt/SnO₂(250H₂) powder were almost metals. XPS spectra of Sn 3d_{5/2} of 2Pt/SnO₂(500air) and 2Pt/SnO₂(250H₂) powders were shown in Fig. S4(a). The valence of Sn species of all the powders was 4+, but the binding energy of Sn 3d_{5/2} of the 2Pt/SnO₂(500air) was larger than that of the 2Pt/SnO₂(250H₂) powder. In addition, the Ar etching slightly shifted the Sn 3d_{5/2} XPS spectrum of the 2Pt/SnO₂(500air) powder to lower binding energy. These results indicate that the heat treatment in H₂ reduced also the valence of the Sn species as well as the Pt species at the surface of the 2Pt/SnO₂(250H₂) powder. XPS spectra of O 1s of 2Pt/SnO₂(500air) and 2Pt/SnO₂(250H₂) powders were also shown in Fig. S4(b). A large peak derived from lattice oxygen species and a small peak derived from adsorbed oxygen species and/or hydroxyl group were confirmed as shown in the O 1s XPS spectra of all the powders. In addition, the Ar etching and the heat treatment in H₂ decreased the amount of adsorbed oxygen species and/or hydroxyl group. These results also support that the valence of Pt and Sn species were reduced by the Ar etching and the heat treatment in H₂.

Transmission electron microscopy (TEM) photographs of 2Pt/SnO₂(500air) and 2Pt/SnO₂(250H₂) powders are shown in Fig. 4. Pt nanoparticles were not confirmed in the photograph of the 2Pt/SnO₂(500air) powder. However, the energy dispersive X-ray spectroscopy (EDS) analysis of this

area showed that the weight ratio of Pt with Sn (Pt : Sn) was 97.8 : 2.2, which indicated that the Pt species certainly mixed with SnO₂. Hübner et al. have investigated the composition and chemical state of thick Pt/SnO₂ films which were fabricated by screen printing, and then they have suggested that the Ptⁿ⁺ species were located at the Sn position in the rutile structure [27]. Murata et al. also have discussed that the relatively large amount of Pt (\leq ca. 10 at%) was doped as Ptⁿ⁺ species into a SnO₂ lattice in the thin Pt-SnO₂ composite films which were fabricated with magnetron sputtering using a Pt/SnO₂ target [28]. Considering their results, the preparation technique of Pt/SnO₂(Tm) powders in this study, and the radii of 6-coordinate ions (Pt⁴⁺: 0.625 Å, Pt²⁺: 0.80 Å, Sn⁴⁺: 0.83 Å),²⁹ it was expected that most of Pt⁴⁺ and Pt²⁺ were doped into the Sn⁴⁺ sites in the lattice at the SnO₂ surface. In addition, a slight number of Pt-based nanoparticles, of which surface had been oxidized to PtO and/or PtO₂, was probably loaded onto the surface of the 2Pt/SnO₂(500air) powder, because the small amount of Pt metal was also confirmed by XPS. On the other hand, (111) planes of Pt metal were confirmed as nanoparticles in the TEM photograph of the 2Pt/SnO₂(250H₂) powder. In addition, clustered Pt species may also exist on the SnO₂ surface, but we could not observe them in the photograph. In addition, the amount of Pt of the 2Pt/SnO₂(250H₂) powder (Pt : Sn = 94.7 : 5.3 in weight), which was measured with EDS, was larger than that of the 2Pt/SnO₂(500air) powder. This difference is probably derived from the physical and chemical states of Pt and SnO₂ and their nanostructure, which must be largely involved in the gas-sensing properties.

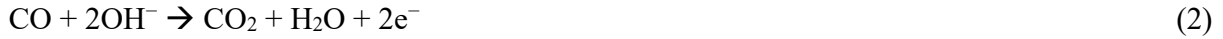
3.2 Electrochemical reaction on sensing-electrode surface

Effects of humidity and oxygen concentration in the target gas on the CO-sensing properties of the EC(2Pt/SnO₂(500air)) sensor have been investigated to clarify the CO-sensing mechanism. Figure 5(a) shows RH dependence of the response to 500 ppm CO balanced with dry or wet synthetic air (RH: 0–80%) at 30°C. The RH of both the target and reference gases was controlled at the same value. The CO responses of the sensor were not so much dependent on RH ($\Delta E_{\text{CO}}(500)$: ca. 100–120 mV), but the moderate humidity (20–40%RH) slightly increased the CO response. In addition, the EC(2Pt/SnO₂(500air)) sensor showed quite large and reasonable response behavior even in dry air, whereas the sensor using Au-loaded SnO₂ sensing electrodes was not able to be operated in dry air [24]. Such difference between both Pt and Au loaded onto SnO₂ may arise from the mechanism of the CO anodic reaction on their surface. In addition, variation in the magnitude of O₂ response (ΔE_{O_2}) of the EC(2Pt/SnO₂(500air)) sensor with O₂ concentration in 500 ppm CO balanced with wet synthetic air on the SE side at 30°C (RH: 57%, CO-free wet synthetic air on the RE side) is shown in Fig. 5(b). The ΔE_{O_2} shifted positively with an

increase in O₂ concentration. This behavior indicates that an electrochemical reaction involving O₂ largely influences the CO-response behavior. We have already discussed the electrochemical CO-sensing mechanism of a potentiometric gas sensor using an ACP electrolyte [24, 25]. The sensing-electrode potential of the EC(2Pt/SnO₂(500air)) sensor in wet synthetic air is generally derived from the oxygen redox reaction as shown below.



On the other hand, the sensor showed negative response to CO and the O₂ concentration largely contributed to their *E* value in wet synthetic air containing CO. Thus, the anodic reaction (eq. (2)) and the cathodic reaction of oxygen (forward reaction of eq. (1)) simultaneously proceed at the surface of the sensing electrode in the gaseous atmosphere, and the mixed potential resulting from electrochemical reactions of eqs. (1) and (2) determines the sensing-electrode potential of the sensor.



Therefore, the *E* value was very sensitive to the change also in the concentration of CO, as shown in Figs. 1 and 2. Since H₂ molecules are also electrochemically oxidized in alkaline media as shown below, the sensing-electrode potential in synthetic air containing H₂ is determined by the mixed potential resulting from both the anodic reaction of H₂ (eq. (3)) and the cathodic reaction of oxygen (forward reaction of eq. (1)).



The EC(2Pt/SnO₂(500air)) sensor showed much larger CO response than H₂ response (i.e., large CO selectivity against H₂, see Figs. 1 and 2), and most of the Pt components were oxidized on the 2Pt/SnO₂(500air) surface (see Fig. 3). These results suggest that the electrocatalytic activity for CO oxidation was much larger than that for H₂ oxidation, just on the surface of oxidized Pt components. On the other hand, the EC(2Pt/SnO₂(250H₂)) sensor showed much larger responses to both CO and H₂ than those of the EC(2Pt/SnO₂(500air)) sensor, and the CO selectivity of the EC(2Pt/SnO₂(250H₂)) sensor against H₂ was much poor than that of the EC(2Pt/SnO₂(250H₂)) sensor (see Figs. 1 and 2). In addition, the Pt components almost existed as a metal on the 2Pt/SnO₂(500air) surface (see Fig. 3), and a part of the SnO₂ surface was reduced (see Fig. 4S). These results imply that the electrocatalytic activities for both CO and H₂ oxidations are really high on the surface of metallic Pt components and the reduced SnO₂ surface may support these electrocatalytic activities of the metallic Pt components.

After these sensors were stored for 3 weeks under normal atmosphere, their CO and H₂ response properties were investigated again. Response transients of 3-week stored EC(2Pt/SnO₂(500air)) and

EC(2Pt/SnO₂(250H₂)) sensors to 10–3000 ppm CO and H₂ were shown in Fig. 6. In addition, Fig. 7 shows concentration dependences of CO and H₂ responses of 3-week stored EC(2Pt/SnO₂(500air)) and EC(2Pt/SnO₂(250H₂)) sensors with their sensitivities to CO and H₂, in wet synthetic air at 30°C (57%RH), together with those of as-fabricated EC(2Pt/SnO₂(500air)) and EC(2Pt/SnO₂(250H₂)) sensors. The storage of the EC(2Pt/SnO₂(500air)) sensor for 3 weeks increased its CO response slightly, together with little effect on the CO sensitivity. However, the H₂ response and sensitivity of the sensor hardly changed even after the 3-week storage. Therefore, the CO selectivity of the sensor against H₂ (ca. $\Delta E_{CO}/\Delta E_{H_2}(500)$: ca. 12.0) was larger than that of the as-fabricated (ca. $\Delta E_{CO}/\Delta E_{H_2}(500)$: ca. 8.3). On the other hand, the 3-week storage of the EC(2Pt/SnO₂(250H₂)) sensor largely decreased their responses and sensitivities to both CO and H₂. Namely, the CO response of the 3-week stored EC(2Pt/SnO₂(250H₂)) sensor was smaller than that of the as-fabricated EC(2Pt/SnO₂(500air)) sensor, and the CO sensitivity of the 3-week stored EC(2Pt/SnO₂(250H₂)) sensor was quite comparable to that of the as-fabricated EC(2Pt/SnO₂(500air)) sensor. The H₂ response and sensitivity of the 3-week stored EC(2Pt/SnO₂(250H₂)) sensor was still larger than those of the as-fabricated EC(2Pt/SnO₂(500air)) sensor, but the 3-week storage certainly reduced both the H₂ response and sensitivity. Therefore, the CO selectivity of the EC(2Pt/SnO₂(250H₂)) sensor against H₂ ($\Delta E_{CO}/\Delta E_{H_2}(500)$: ca. 2.7) was slightly larger than that of the as-fabricated EC(2Pt/SnO₂(250H₂)) sensor ($\Delta E_{CO}/\Delta E_{H_2}(500)$: ca. 1.9), but the value was much smaller than that of the EC(2Pt/SnO₂(500air)) sensor. These results show that the heat treatment in H₂ at 250°C for 1 h was quite effective in enhancing both the sensing properties to both CO and H₂, but the effectiveness reduced even after short storage in ambient air. This is probably because the metallic Pt and/or reduced SnO₂ components on the 2Pt/SnO₂(250H₂) surface were slightly oxidized during the 3-week storage in ambient air. In addition, the physical and chemical surface states (morphology and composition) of the 2Pt/SnO₂(250H₂) powder after 3-week storage in ambient air seem to be completely different from those of the 2Pt/SnO₂(500air) powder. Namely, the surface of Pt nanoparticles, which were deposited by the heat treatment in H₂ at 250°C, were oxidized and/or the covering of the active sites on the Pt surface with other components may deactivated the electrocatalytic properties for CO oxidation. Now, the investigation of the chemical state of their surface by XPS is quite effective in clarifying the change in the sensing behavior. However, it is really difficult to do that, because the 2Pt/SnO₂(250H₂) powder were completely mixed with ACP to form the sensing electrode. Hereafter, it is indispensable to analyze the change in the chemical and physical states of the electrode surface by using various *in-situ* or *operando* technique.

3.3 Effects of the amount of Pt loading on CO-sensing properties of EC(*n*Pt/SnO₂(500air)) sensors

The enhancement in the CO-sensing properties and the clarification of the gas-sensing mechanism have been attempted by controlling the amount of Pt loaded onto SnO₂. Figures S5, S6, and S7(a) show response transients of the as-fabricated EC(*n*Pt/SnO₂(500air)) sensors (*n*: 0.1, 0.5, 5, 7, 10) to CO and H₂ balanced with wet synthetic air at 30°C (57%RH), and Fig. 8 summarizes concentration dependences of the responses to CO and H₂ and variations in responses to 500 ppm CO and H₂, sensitivity to CO and H₂, and CO selectivity against H₂ ($\Delta E_{CO}/\Delta E_{H_2}(500)$) with the amount of Pt loaded onto SnO₂, in wet synthetic air (57%RH) at 30°C. The loading of the small amount of Pt loaded (0.1 wt%) onto SnO₂ was hardly effective in improving responses of the EC(SnO₂) sensor to both 500 ppm CO and 500 ppm H₂, and thus concentration dependence of CO and H₂ responses of the EC(0.1Pt/SnO₂(500air)) sensor was not investigated in this study. The increase in the amount of Pt loaded to 0.5 wt% drastically enhanced only the CO response and sensitivity, while maintaining the small H₂ response and sensitivity. Thus, the CO selectivity of the EC(0.5Pt/SnO₂(500air)) sensor against H₂ was the largest among all the EC(*n*Pt/SnO₂(500air)) sensors. However, the response and recovery speeds to both CO and H₂ were quite slow, as shown in Fig. S5(b). The further increase in the amount of Pt loaded onto SnO₂ up to 5.0 wt% largely improved the response and recovery speeds. In addition, it slightly enhanced the H₂ response and sensitivity, without considerable increment in the CO response and sensitivity, and thus the CO selectivity against H₂ slightly decreased with an increase in the amount of Pt loaded. However, the Pt loading over 7.0 wt% drastically improved the H₂ response and sensitivity while the CO response and sensitivity remained unchanged, and thus their sensors showed extremely small CO selectivity against H₂. In addition, response transients of the EC(10Pt/SnO₂(500air)) sensor to CO and H₂ were measured after 13-week storage in ambient air as shown in Fig. S7(b), and Fig. S7(c) summarizes concentration dependences of CO and H₂ responses of the as-fabricated and 13-week stored EC(10Pt/SnO₂(500air)) sensor. The CO response (e.g., $\Delta E_{CO}(500)$): ca. 135 mV) and the CO sensitivity (ca. 50 mV/decade) of the 13-week stored EC(10Pt/SnO₂(500air)) sensor were comparable to those of the as-fabricated EC(10Pt/SnO₂(500air)) sensor. On the other hand, the H₂ response of the 13-week stored EC(10Pt/SnO₂(500air)) sensor (e.g., $\Delta E_{H_2}(500)$): ca. 92 mV) was smaller than that of the as-fabricated EC(10Pt/SnO₂(500air)) sensor and thus the CO selectivity against H₂ increased up to ca. 1.47 after the 13-week storage, while the H₂ sensitivity of the 13-week stored EC(10Pt/SnO₂(500air)) sensor (ca. 52 mV/dec) was comparable to that of the as-fabricated EC(10Pt/SnO₂(500air)) sensor.

To clarify the reason why the gas-sensing properties are largely dependent on the amount of Pt loaded onto SnO₂, the XRD analysis and N₂ adsorption-desorption measurement of typical *n*Pt/SnO₂(500air)

powders have been attempted in this study. The XRD spectra of their powders were shown in Fig. S8, together with their crystallite size. The XRD peaks of SnO₂ hardly shift by the loading of the small amount of Pt (*n*: 0.1 and 0.5), also as described in Fig. S2, whereas the loading of the large amount of Pt (*n*: 5.0 and 10) obviously shifted the XRD peaks to lower angle. Namely, the d-spacing calculated from (110) plane of the pristine SnO₂ powder (Fig. S2(a)) is 3.357 Å, while those of the 5Pt/SnO₂(500air) and 10Pt/SnO₂(500air) powders were 3.410 Å and 3.412 Å, respectively. Considering that the size of Pt⁴⁺ and Pt²⁺ (0.625 Å and 0.80 Å in radius (6-coordinate), respectively) is smaller than that of Sn⁴⁺ (0.83 Å in radius (6-coordinate)) [29], the increase in the d-spacing is probably derived from the production of oxygen vacancies in the SnO₂ lattice, which are induced by the doping of Pt components (especially Pt²⁺). Furthermore, N₂ adsorption-desorption isotherms and pore size distributions of these powders, together with their specific surface areas (SSA) are shown in Fig. S9, but the SSA value almost remained unchanged even by the loading of 10 wt% Pt and the subsequent heat-treatment in air (cf. Fig. S3(i)).

Furthermore, Fig. 9 shows XPS spectra of Pt 4f of typical *n*Pt/SnO₂(500air) powders (*n*: 0.1, 0.5, 5.0, 10), and variations in the ratio of each Pt component to total Pt and SnO₂ with the amount of Pt loaded onto SnO₂ are shown in Fig. S10, together with the ratio of total Pt to SnO₂. All the ratios were calculated by deconvolution of their XPS spectra. In addition, XPS spectra of Sn 3d_{5/2} and O 1s of these powders are also shown in Figs. S11 and S12, respectively. The 0.1Pt/SnO₂(500air) powder hardly had Pt metal, and its Pt component consisted of only the large amount of Pt⁴⁺ (ca. 84.2%) and the small amount of Pt²⁺. These oxidized Pt components were probably doped just into the SnO₂ lattice, also as discussed in the preceding section. The ratio of Pt²⁺ and Pt metal to total Pt increased and the ratio of Pt⁴⁺ decreased with an increase in the amount of Pt loaded onto SnO₂ up to 2 wt%. However, the increase in the amount of Pt loaded over 2 wt% increased the ratio of Pt⁴⁺ and decreased the ratio of Pt²⁺ with almost the same ratio of Pt metal, while the ratio of total Pt to SnO₂ slightly increased with an increase in the amount of Pt loaded onto SnO₂ in the whole range. These results strongly indicate that the surface chemical state of the *n*Pt/SnO₂(500air) powders largely changed beyond the amount of Pt loaded of 2 wt%, probably because Pt components deposited on SnO₂ (e.g., largely surface-oxidized Pt-based nanoparticles) began to subject the chemical properties of the surface. Moreover, the XPS peaks of Sn 3d_{5/2} and O 1s of these powders gradually shifted to the higher binding energy and the ratio of adsorbed oxygen species and/or hydroxyl group to the lattice oxygen also gradually decreased, with an increase in the amount of Pt loaded onto SnO₂ (especially 5.0 and 10 wt%). Considering that the XRD results indicate that the increase in the amount of Pt increased the amount of oxygen vacancies, the electronic interaction between the Pt species and SnO₂ were relatively strong and the electron density of Pt species of the *n*Pt/SnO₂(500air)

powders increased by the electron transfer from SnO₂ with an increase in the amount of Pt loaded. The gas-sensing mechanism to both CO and H₂ of the EC(*n*Pt/SnO₂(500air)) sensors is discussed in detail in the following section.

The 10Pt/SnO₂(250H₂) powder was also prepared, and its physical properties were investigated by XRD and N₂ adsorption-desorption, as shown in Fig. S13. Several peaks derived from Pt and PtSn were confirmed in the XRD spectrum. In addition, the d-spacing of SnO₂ of the powder is smaller than that of the 10Pt/SnO₂(500air) powder. This is probably because the oxygen vacancies, which were relatively stable at 500°C in air, reduced with the reduction in SnO₂ to Sn and the subsequent alloying of Pt with Sn at 250°C in H₂, due to the large amount of Pt loaded. The crystallite size of the 10Pt/SnO₂(250H₂) powder is comparable to that of the 10Pt/SnO₂(500air) powder. The pore-size distribution and the specific surface area of the 10Pt/SnO₂(250H₂) powder were also comparable to those of the 10Pt/SnO₂(500air) powder. The responses of as-fabricated and 3-week stored EC(10Pt/SnO₂(250H₂)) sensor to 500 ppm CO and H₂ were simply investigated in wet synthetic air at 30°C, as shown in Fig. S14. The CO and H₂ responses of the as-fabricated sensor was ca. 252 mV and 158 mV, respectively, and the both values and the CO selectivity against H₂ ($\Delta E_{CO}/\Delta E_{H_2}(500)$: ca. 1.59) were much larger than those of the EC(10Pt/SnO₂(500air)) sensor. The storage of the sensor for 3 weeks enhanced both the CO and H₂ responses (ca. 310 mV and ca. 206 mV, respectively, when maintaining the CO selectivity against H₂ ($\Delta E_{CO}/\Delta E_{H_2}(500)$: ca. 1.50). The effect of the short-term storage on the gas-sensing properties was largely different from those of the EC(*n*Pt/SnO₂(500air)) sensors (*n*: 0.2 and 10, see Figs. 7 and S7, respectively). These differences are expectantly associated with the generation of PtSn alloy, but presently we cannot find how the PtSn alloy influences the gas-sensing properties. Anyway, the large amount of Pt loaded onto SnO₂ and the subsequent heat treatment in H₂ at elevated temperatures were effective in enhancing the response to both CO and H₂ and the long-term stability, and thus various treatments to the electrode materials, co-loading of Pt and other catalysts, and other modifications will be hereafter attempted to improve the CO-sensing properties.

3.4 Gas-sensing mechanism of EC(*n*Pt/SnO₂(500air)) sensors

On the basis of all results in this paper, we can draw schematic diagrams of current-potential characteristics, or polarization curves for related electrochemical reactions (oxygen cathodic reaction as well as CO and H₂ anodic reactions) of the sensing electrodes of the EC(*n*Pt/SnO₂(500air)) sensors, as shown in Fig. 10. In this figure, the intersections of these anodic and cathodic reactions (namely, closed circles)

just mean mixed potentials of the sensing electrodes. According to these diagrams, we can easily understand that the higher CO-anodic activity or lower O₂-cathodic activity is indispensable for the large CO response and the higher CO-anodic activity or lower H₂-anodic activity is essential for the excellent CO selectivity, and we actually succeeded to enhance the CO-sensing properties (CO response as well as CO selectivity against H₂) of the EC(*n*Pt/SnO₂(500air) sensors by controlling the amount of Pt loaded onto SnO₂, as shown above. The slope of the polarization curves of the oxygen cathodic reactions decreases with an increase in the amount of Pt loaded, because the Pt species are well known as an excellent electrocatalyst for oxygen reduction and thus the overpotential for oxygen reduction gradually reduces with an increase in the amount of Pt loaded. In addition, the slope was expected to be independent of the kind of target gas (namely, CO or H₂). However, the variations in the responses with the amount of Pt loaded onto SnO₂ was largely dependent on the kind of target gas. The EC(0.1Pt/SnO₂(500air) sensor showed extremely small CO response, but the CO response abruptly increased with an increase in the amount of Pt loaded up to 0.5 wt%. This behavior indicates that the CO-anodic activity drastically increased and thus the overpotential drastically reduced with a slight increase in the amount of Pt, especially from 0.1 wt% to 0.5 wt%. Therefore, the mixed potential resulting from CO oxidation and O₂ reduction largely shifted to the negative direction and thus the CO response also drastically increased, with a slight increase in the amount of Pt loaded in the range, as shown in Fig. 10(a). Further increase in the amount of Pt loaded enhanced also the oxygen cathodic activity as well as the CO cathodic activity. Therefore, the mixed potential gradually shifted to the negative direction and thus the CO response only gradually enhanced with an increase in the amount of Pt loaded.

The possible process of the CO anodic reaction on the electrode surface is shown in Fig. S15(a), also on the basis of the XPS results (see Fig. 3 and 9). When the small amount of Pt was loaded on SnO₂ surface, it is strongly expected that most of the Pt are mono-dispersively doped at the surface SnO₂ lattice, on the basis of these results in this study and Pt doping into SnO₂ lattice structure which was suggested by Hübner et al. [27] or Murata et al. [28]. CO molecules can easily adsorb over the mono-dispersive Pt species, and thus CO molecules are easily oxidized even by the small amount of Pt loaded. On the other hand, oxygen molecules also can adsorb over the mono-dispersive Pt species, but the oxygen cathodic activity on the surface seems not to be rather activated than the CO anodic activity, considering the effect of the amount of Pt loading onto SnO₂ on the CO-sensing properties (see Fig. 8). The slight increase in the amount of Pt loaded enhanced the CO anodic activity, which causes the reduction in the overpotential, the abrupt shift of the mixed potential to the negative direction, and then the improvement of the CO response. When the large amount of Pt (over 0.5 wt%) was loaded on SnO₂ surface, however, surface-

oxidized Pt-based nanoparticles (agglomerates, PtOx/Pt) produced on SnO₂ surface, on the basis of the XPS result. On the PtOx/Pt surface, the oxygen cathodic reaction as well as CO anodic reaction easily proceeded simultaneously, and both the overpotential for CO oxidation and oxygen reduction decreased with an increase in the amount of Pt loaded, considering the effect of the amount of Pt loading onto SnO₂ on the CO-sensing properties. Therefore, the large amount of Pt loaded (over 0.5 wt%) realized the large CO response of the EC(*n*Pt/SnO₂(500air)) sensors, but the increase in the amount of Pt loaded did not have a significant effect on the magnitude of CO response.

On the other hand, the EC(0.1Pt/SnO₂(500air)) sensor hardly showed the H₂ response, too, and the H₂ response slightly increased with an increase in the amount of Pt loaded in the range of 0.5 to 5.0 wt% (see Fig. 8). These results indicate that the H₂-anodic activity hardly increased (namely, the overpotential hardly reduced) and thus the mixed potential resulting from H₂ oxidation and O₂ reduction also hardly shifted to the negative direction with an increase in the amount of Pt in the range, as shown in Fig. 10(b). Therefore, the EC(*n*Pt/SnO₂(500air)) sensors (*n*: 0.5–5.0) showed excellent CO sensitivity against H₂. However, the H₂-anodic activity drastically increased and thus the overpotential for H₂ oxidation drastically reduced with a large increase in the amount of Pt from 5 to 10 wt%. Therefore, the H₂ response drastically increased and thus the CO selectivity against H₂ became quite small with an increase in the amount of Pt of over 5 wt%. The possible process resulting from these electrochemical reactions is shown in Fig. S15(b). When the small amount of Pt was loaded on SnO₂ surface, H₂ molecules are quite difficult to adsorb over the mono-dispersive Pt species, and thus both the H₂ anodic and oxygen cathodic activity are really low on the surface. Therefore, the overpotential for H₂ oxidation is quite large in the *n* range of less than 5.0 (wt%), and thus the mixed potential only slightly shifted and their H₂ response is quite low. However, H₂ molecules can quite easily adsorb dissociatively on the PtOx/Pt surface. This means that the H₂ anodic activity are easily oxidized even by the large amount of Pt loaded. Therefore, the increase in the amount of Pt loaded over 5 wt% enhanced the H₂ anodic activity, which causes the reduction in the overpotential, the abrupt shift of the mixed potential to the negative direction, and then the improvement of the H₂ response.

Presently, we do not have the clear evidence for the electrochemical mechanism of the CO and H₂-sensing properties of the EC(*n*Pt/SnO₂(500air)) sensors, because the ionic conductivity of the ACP electrolyte and/or the electron conductivity of the *n*Pt/SnO₂(500air) electrodes are too low to measure the polarization properties of the related electrochemical reactions as shown in eqs. (1)–(3). Hereafter, the improvements of these problems and the implementation of the measurement of the polarization properties are the important keys to clarify the gas-sensing mechanism.

4. CONCLUSION

CO-sensing properties of EC(n Pt/SnO₂(T_m)) sensors have been investigated mainly at 30°C in wet synthetic air (57%RH), and their CO-sensing mechanism has been discussed in this paper, by controlling the amount of Pt loaded onto SnO₂ and the subsequent heat-treatment conditions. The EC(n Pt/SnO₂(500air)) sensors showed the large CO response in the n range of over 0.5 (wt%), while their H₂ response was quite small in the n range of up to 5.0 (wt%). Thus, their CO selectivity against H₂ was relatively large in the n range of 0.5–5.0 (wt%). The magnitude of their CO responses was not so much dependent on the humidity, and the sensing-electrode potential was governed by mixed potential resulting from electrochemical CO (or H₂) oxidation and O₂ reduction, on the basis of the oxygen-concentration dependence and CO (or H₂)-concentration dependences on their responses. Most of Pt loaded onto SnO₂ was oxidized to form PtOx and the significant proportion of Pt species seems to be dispersively doped at the surface SnO₂ lattice. Especially, CO molecules were efficiently anodized even on the mono-dispersive and oxidized Pt species as an active site, while H₂ molecules were quite difficult to be electrochemically oxidized on them. This electrocatalytic properties of the Pt-based active sites is the most considerable reason why the EC(n Pt/SnO₂(500air)) sensors showed the excellent CO selectivity against H₂ in the n range of 0.5–5.0 (wt%). However, the large amount of Pt loaded onto SnO₂ increased the surface-oxidized Pt-based nanoparticles (agglomerates, PtOx/Pt) on SnO₂ surface. As the anodic reaction of H₂ as well as CO easily and simultaneously proceeded on the PtOx/Pt surface, both the CO and H₂ responses are quite large and thus the CO selectivity against H₂ was quite low. On the other hand, the heat treatment at 250°C in H₂ after the Pt loading also enhanced both CO and H₂ responses and thus decreased the CO selectivity against H₂, because of the reduced surface of Pt-loaded SnO₂. The large number of metallic Pt species produced on the surface easily anodized CO as well as H₂, and thus the CO and H₂ responses of the EC(n Pt/SnO₂(250H₂)) sensors were much larger than those of the EC(n Pt/SnO₂(500air)) sensors and they showed quite low CO selectivity against H₂.

APPENDIX

List of all symbols.

Symbol	Description and definition
ACP	Anion-conducting polymer
$n\text{Pt}/\text{SnO}_2(T_m)$	n wt% Pt-loaded SnO_2 powder prepared by precipitation-deposition technique (T : heat-treatment temperature ($^{\circ}\text{C}$), m : heat-treatment atmosphere (air or H_2))
CS	Crystallite size calculated from XRD pattern by using Scherrer equation
$\Delta E_{\text{CO}}/\Delta E_{\text{H}_2}(c)$	CO selectivity against H_2 (ratio of CO response to H_2 response, c : concentration (ppm))
ΔE_{SG} or $\Delta E_{\text{SG}}(c)$	The magnitude of response to SG (SG: sample gas, CO or H_2 , c : concentration (ppm))
E	Electromotive force (mV)
EC(EM)	Sensor element (EC: electrochemical cell, EM: electrode material (SnO_2 or $n\text{Pt}/\text{SnO}_2(T_m)$))
S_{SG}	Sensitivity to CO or H_2 (slope of relationship between the magnitude of response to sample gas (CO or H_2) and the logarithm of the concentration)
SSA	Specific surface area ($\text{m}^2 \text{g}^{-1}$)
T_{RC}	90% recovery time (period necessary to reach 90% value of ΔE_{SG} from E value in a sample gas)
T_{RS}	70% response time (period necessary to reach 70% value of ΔE_{SG} from E value in a base gas)

REFERENCES

- (1) Ishiji, T.; Takahashi, K.; Kira, A. Amperometric carbon dioxide gas sensor based on electrode reduction of platinum oxide, *Anal. Chem.* **1993**, 65, 2376–2739.
- (2) Takahashi, M.; Ishiji, T.; Kawashima, N. Handmade oxygen and carbon dioxide sensors for monitoring the photosynthesis process as instruction material for science education, *Sens. Actuators B* **2001**, 77, 237–243.
- (3) Imaiya, H.; Okamura, K.; Nakano, N.; Nagashima, K.; Suzuki, Y.; Takahashi, K. Development of electrochemical CO gas sensor using expanded polytetrafluoroethylene membrane modified by ion implantation, *Electrochemistry* **2011**, 79, 140–145.
- (4) Obermeier, J.; Trefz, P.; Wex, K.; Sabel, B.; Schubert, J. K.; Miekisch, W. Electrochemical sensor system for breath analysis of aldehydes, CO and NO, *J. Breath Res.* **2015**, 9, 016008.
- (5) Yamazoe, N.; Hisamoto, J.; Miura, N. Solid-state oxygen sensor using sputtered LaF₃ film, *Sens. Actuators* **1987**, 12, 415–423.
- (6) Miura, N.; Yamazoe, N. Development of new chemical sensors based on low-temperature proton conductors, *Solid State Ionics* **1992**, 53-56, 975–982.
- (7) Toniolo, R.; Bortolomeazzi, R.; Svirgelj, R.; Dossi, N.; Casella, I. G.; Bragato, C.; Daniele, S. Use of an electrochemical room temperature ionic liquid-based microprobe for measurements in gaseous atmosphere, *Sens. Actuators B* **2017**, 240, 239–247.
- (8) Wan, H.; Yin, H.; Mason, A. J. Rapid measurement of room temperature ionic liquid electrochemical gas sensor using transient double potential amperometry, *Sens. Actuators B* **2017**, 242, 658–666.
- (9) Miura, N.; Kato, H.; Yamazoe, N.; Seiyama, T. A proton conductor gas sensor operative at ordinary temperature, *Denki Kagaku (presently Electrochemistry)* **1982**, 50, 858–859.
- (10) Gao, Y.; Kita, H.; Watanabe, Y.; Sima, K. An electrochemical Nafion matrix oxygen sensor and the evaluation of oxygen permeation in coated films, *J. Appl. Electrochem.* **1993**, 23, 1102–1106.
- (11) Mochizuki, K.; Kikuchi, T.; Sudoh, M.; Ishiguro, Y.; Suzuki, T. Performances of fuel-cell-type CO sensors using each of polybenzimidazole and Nafion membranes, *J. Electrochem. Soc.* **2011**, 158, J71–J75.

- (12) Guan, Y.; Dai, M.; Liu, T.; Liu, Y.; Liu, F.; Liang, X.; Suo, H.; Sun, P.; Lu, G. Effect of the dispersants on the performance of fuel cell type CO sensor with Pt–C/Nafion electrodes, *Sens. Actuators B* **2016**, 230, 61–69.
- (13) Guan, Y.; Liu, F.; Wang, B.; Yang, X.; Liang, X.; Suo, H.; Sun, P.; Sun, Y.; Ma, J.; Zheng, J.; Wang, Y.; Lu, G. Highly sensitive amperometric Nafion-based CO sensor using Pt/C electrodes with different kinds of carbon materials, *Sens. Actuators B* **2017**, 239, 696–703.
- (14) Izawa, K.; Introduction of carbon monoxide gas sensors and their application, *Chemical Sensors* **2018**, 34, 8–13.
- (15) Asazawa, K.; Yamada, K.; Tanaka, H.; Oka, A.; Taniguchi, M.; Kobayashi, T. A platinum-free zero-carbon-emission easy fuelling direct hydrazine fuel cell for vehicles, *Angew. Chem. Int. Ed.* **2007**, 46, 8024–8027.
- (16) Yanagi, H.; Fukuda, K. Anion exchange membrane and ionomer for alkaline membrane fuel cells (AMFCs), *ECS Transactions* **2008**, 16(2), 257–262.
- (17) Fukuda, K.; Inoue, H.; Watanabe, S.; Yanagi, H. In-situ observation of CO₂ through the self-purging in alkaline membrane fuel cell (AMFC), *ECS Transactions* **2009**, 19(31), 23–27.
- (18) Unlu, M.; Zhou, J.; Kohl, P. A. Anion exchange membrane fuel cells: Experimental comparison of hydroxide and carbonate conductive ions, *J. Electrochem. Soc.* **2009**, 12, B27–B30.
- (19) Matsumoto, K.; Fujigaya, T.; Yanagi, H.; Nakashima, N. Very high performance alkali anion-exchange membrane fuel cells, *Adv. Funct. Mater.* **2011**, 21, 1089–1094.
- (20) Hyodo, T.; Ishibashi, C.; Matsuo, K.; Kaneyasu, K.; Yanagi, H.; Shimizu, Y. CO and CO₂ sensing properties of electrochemical gas sensors using an anion-conducting polymer as an electrolyte, *Electrochim. Acta* **2012**, 82, 19–25.
- (21) Hyodo, T.; Ishibashi, C.; Yanagi, H.; Kaneyasu, K.; Shimizu, Y. Potentiometric hydrogen sensors using an anion-conducting polymer as an electrolyte, *Reports of the Faculty of Engineering, Nagasaki University* **2012**, 42, 42–47.
- (22) Goto, T.; Hyodo, T.; Kaneyasu, K.; Yanagi, H.; Shimizu, Y. CO sensing properties of electrochemical gas sensors using an anion-conducting polymer as an electrolyte, *ECS Trans.* **2013**, 50(12), 267–272.
- (23) Goto, T.; Hyodo, T.; Ueda, T.; Kamada, K.; Kaneyasu, K.; Shimizu, Y. CO-sensing properties of potentiometric gas sensors using an anion-conducting polymer electrolyte and Au-loaded metal oxide electrodes, *Electrochim. Acta* **2015**, 166, 232–243.

- (24) Hyodo, T.; Goto, T.; Ueda, T.; Kaneyasu, K.; Shimizu, Y. Potentiometric carbon monoxide sensors using an anion-conducting polymer electrolyte and Au-loaded SnO₂ electrodes, *J. Electrochem. Soc.* **2016**, *163*, B300–B308.
- (25) Hyodo, T.; Takamori, M.; Goto, T.; Ueda, T.; Shimizu, Y. Potentiometric CO sensors using anion-conducting polymer electrolyte: Effects of the kinds of noble metal-loaded metal oxides as sensing-electrode materials on CO-sensing properties, *Sens. Actuators B* **2019**, *287*, 42–52.
- (26) K. S. W. Sing, Reporting physisorption data for gas/solid systems with special reference to the determination of surface area and porosity, *Pure Appl. Chem.* **1982**, *54*, 2201–2218.
- (27) Hübner, M.; Koziej, D.; Bauer, M.; Barsan, N.; Kvashnina, K.; Rossell, M. D.; Weimar, U.; Grunwaldt, J.-D. The structure and behavior of platinum in SnO₂-based sensors under working conditions, *Angew. Chem. Int. Ed.* **2011**, *50*, 2841–2844.
- (28) Murata, N.; Suzuki, T.; Kobayashi, M.; Togoh, F.; Asakura, K. Characterization of Pt-doped SnO₂ catalyst for a high-performance micro gas sensor, *Phys. Chem. Chem. Phys.* **2013**, *15*, 17938–17946.
- (29) Shannon, R. D. Revised effective ionic radii and systematic studies of interatomic distances in halides and chalcogenides, *Acta Cryst.* **1976**, *A32*, 751–767.

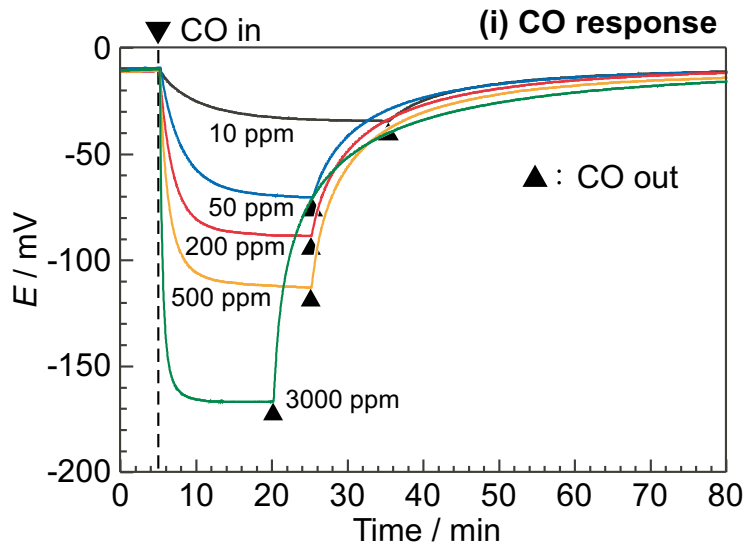
Figure captions

- Figure 1. Response transients of EC(2Pt/SnO₂(500air)) and EC(2Pt/SnO₂(250H₂)) sensors to CO and H₂ in wet synthetic air at 30°C (57%RH).
- Figure 2. Concentration dependences of CO and H₂ responses (ΔE_{SG}) of EC(2Pt/SnO₂(500air)) and EC(2Pt/SnO₂(250H₂)) sensors in wet synthetic air at 30°C (57%RH), together with their sensitivity to CO and H₂ (S_{SG}).
- Figure 3. XPS spectra of Pt 4f of 2Pt/SnO₂(500air) and 2Pt/SnO₂(250H₂) powders. The Pt 4f of 2Pt/SnO₂(500air) powder was analyzed also after Ar etching.
- Figure 4. TEM photographs of 2Pt/SnO₂(500air) and 2Pt/SnO₂(250H₂) powders.
- Figure 5. (a) Variation in ΔE_{CO} of 2Pt/SnO₂(500air) sensor in synthetic air with relative humidity (RH) and (b) variation in ΔE_{O_2} of 2Pt/SnO₂(500air) sensor in 500 ppm CO (57%RH) with O₂ concentration at 30°C.
- Figure 6. Response transients of 3-week stored EC(2Pt/SnO₂(500air)) and EC(2Pt/SnO₂(250H₂)) sensors to (a) CO and (b) H₂ in wet synthetic air at 30°C (57%RH).
- Figure 7. Concentration dependences of CO and H₂ responses (ΔE_{SG}) of as-fabricated and 3-week stored EC(2Pt/SnO₂(500air)) and EC(2Pt/SnO₂(250H₂)) sensors in wet synthetic air at 30°C (57%RH), together with their sensitivities to CO and H₂ (S_{SG}).
- Figure 8. (a) Concentration dependences of ΔE_{CO} and ΔE_{H_2} of n Pt/SnO₂(500air) sensors in wet synthetic air at 30°C (57%RH) and (b) variations in their responses to 500 ppm CO and H₂, sensitivities to CO and H₂ (S_{SG}), and CO selectivity against H₂ ($\Delta E_{CO}/\Delta E_{H_2}(500)$).
- Figure 9. XPS spectra of Pt 4f of typical n Pt/SnO₂(500air) powders (n : 0.1, 0.5, 5.0, 10).
- Figure 10. Schematic drawings of current-potential characteristics (polarization curves) for oxygen cathodic reaction as well as CO and H₂ anodic reactions of the sensing electrodes of the EC(n Pt/SnO₂(500air)) sensors (a) in CO and (b) in H₂ balanced with wet air. EP_{air} and EP_{MP} shows electrode potentials in air and in CO or H₂ balanced with wet air, respectively, and the open circles show mixed potential of their sensing electrodes (namely, EP_{MP}).

Table 1. Typical 90% response time (T_{RS}) and 70% recovery time (T_{RC}) of EC(2Pt/SnO₂(500air)) and EC(2Pt/SnO₂(250H₂)) sensors to CO and H₂.

Sensor	Target gas	T_{RS} / min		T_{RC} / min	
		10 ppm	3000 ppm	10 ppm	3000 ppm
EC(2Pt/SnO ₂ (500air))	CO	13.5	1.8	13.2	8.2
	H ₂	26.0	13.0	31.0	13.5
EC(2Pt/SnO ₂ (250H ₂))	CO	8.8	2.8	14.0	2.2
	H ₂	3.8	1.2	2.2	1.6

(a) EC(2Pt/SnO₂(500air)) sensor



(b) EC(2Pt/SnO₂(250H₂)) sensor

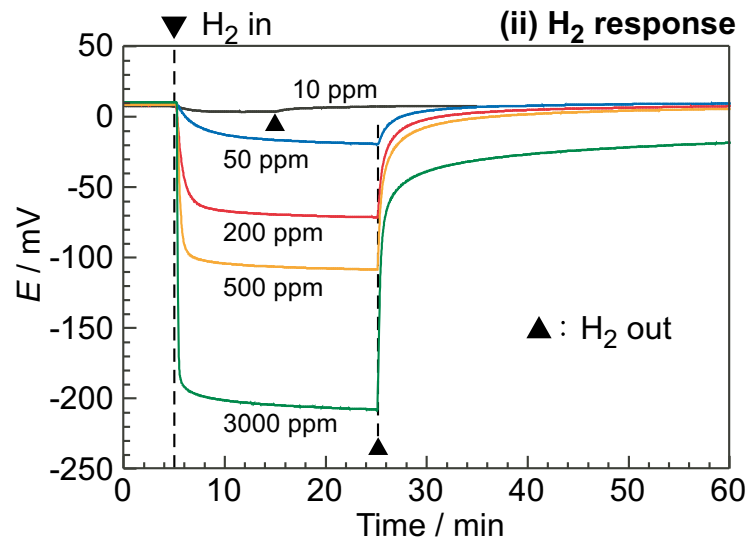
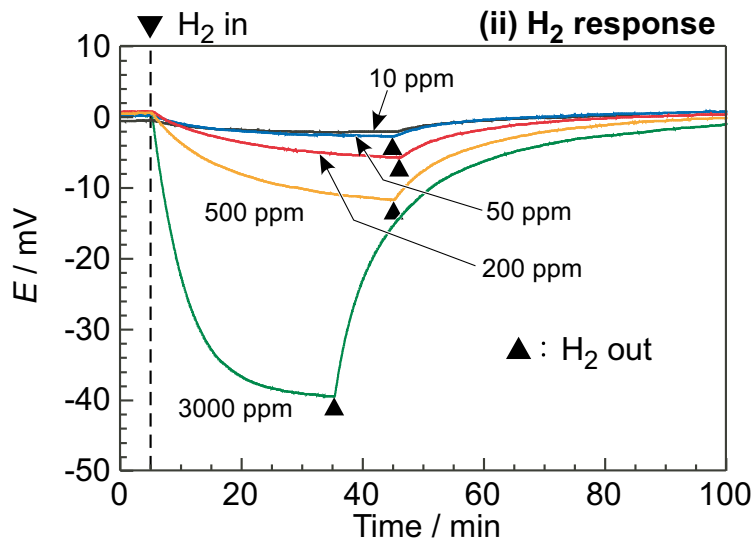
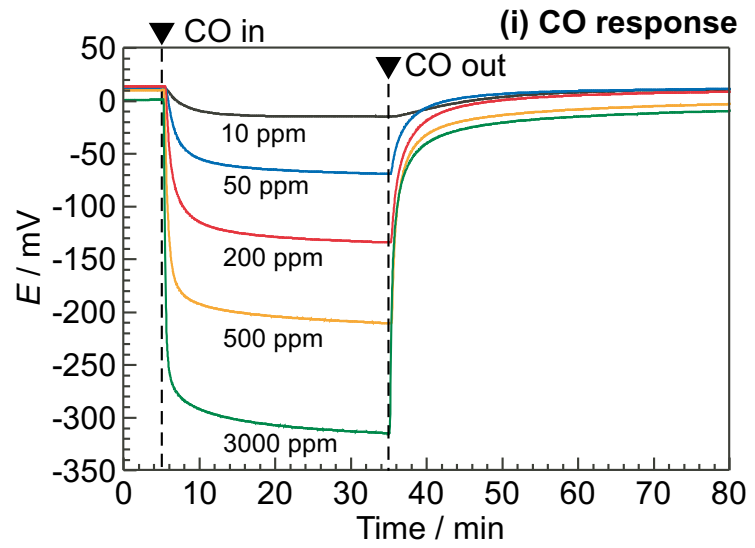


Fig. 1. Hyodo et al.

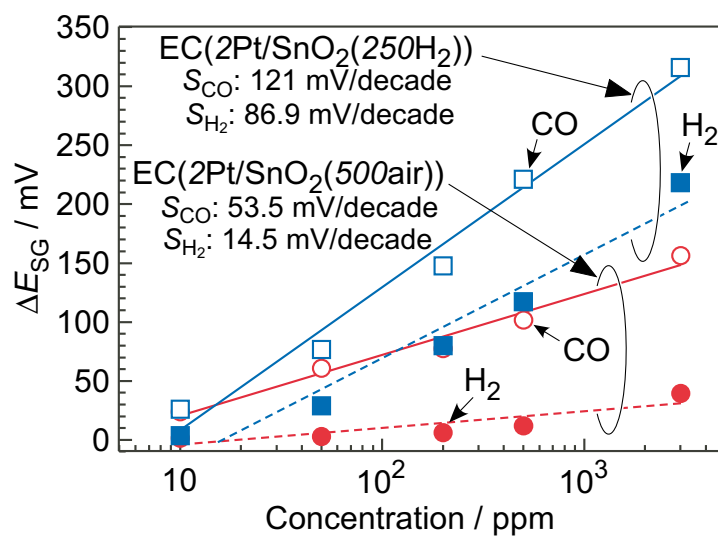


Fig. 2. Hyodo et al.

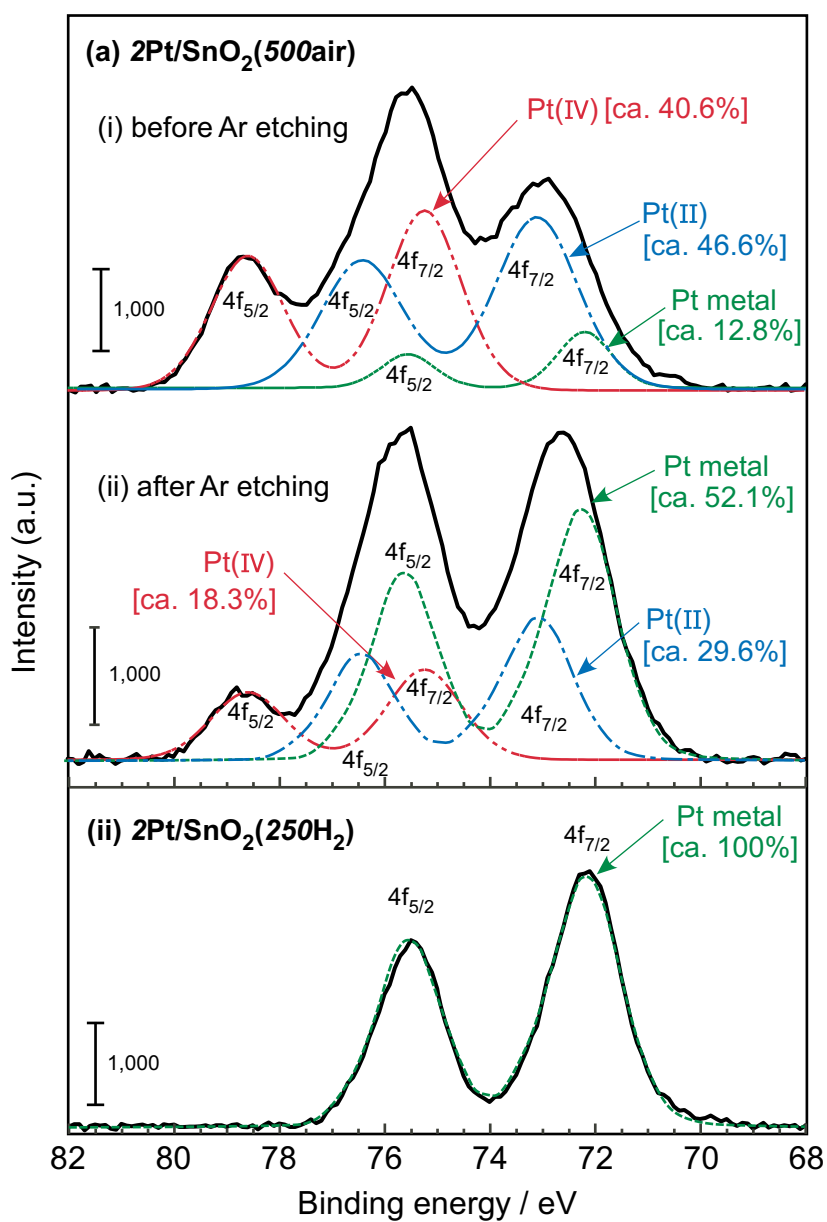


Fig. 3. Hyodo et al.

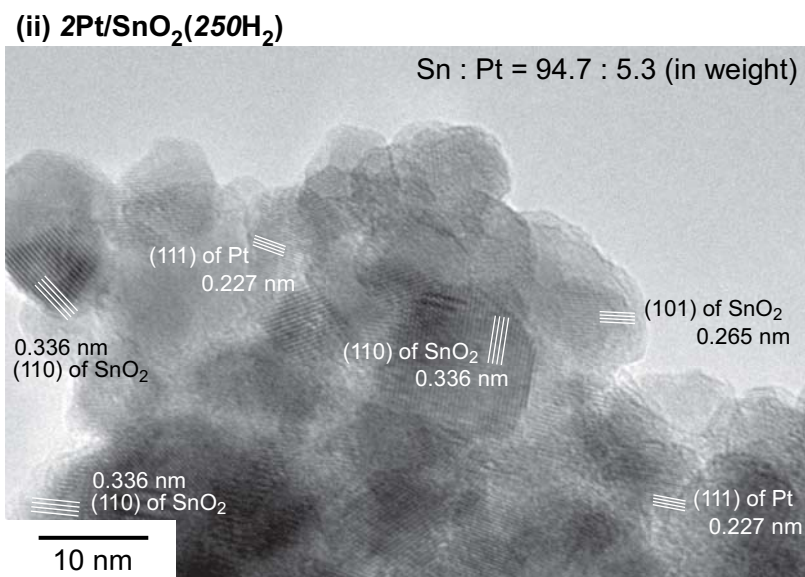
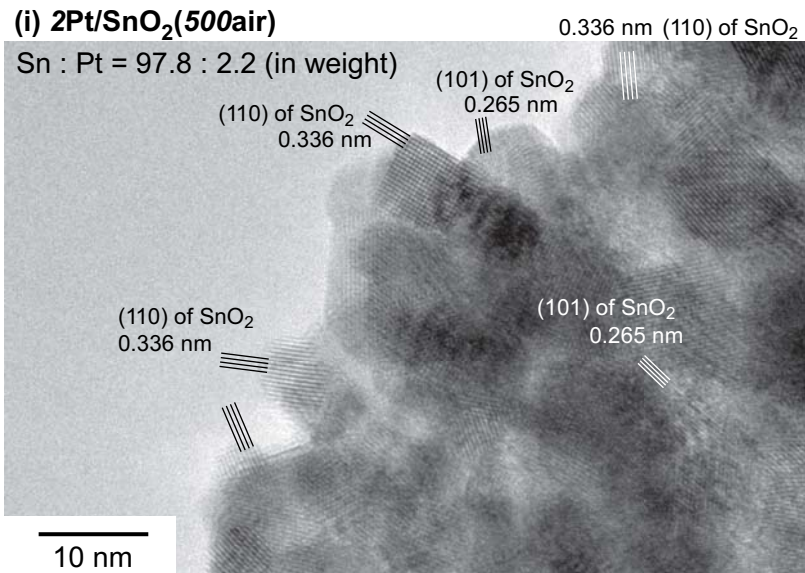


Fig. 4. Hyodo et al.

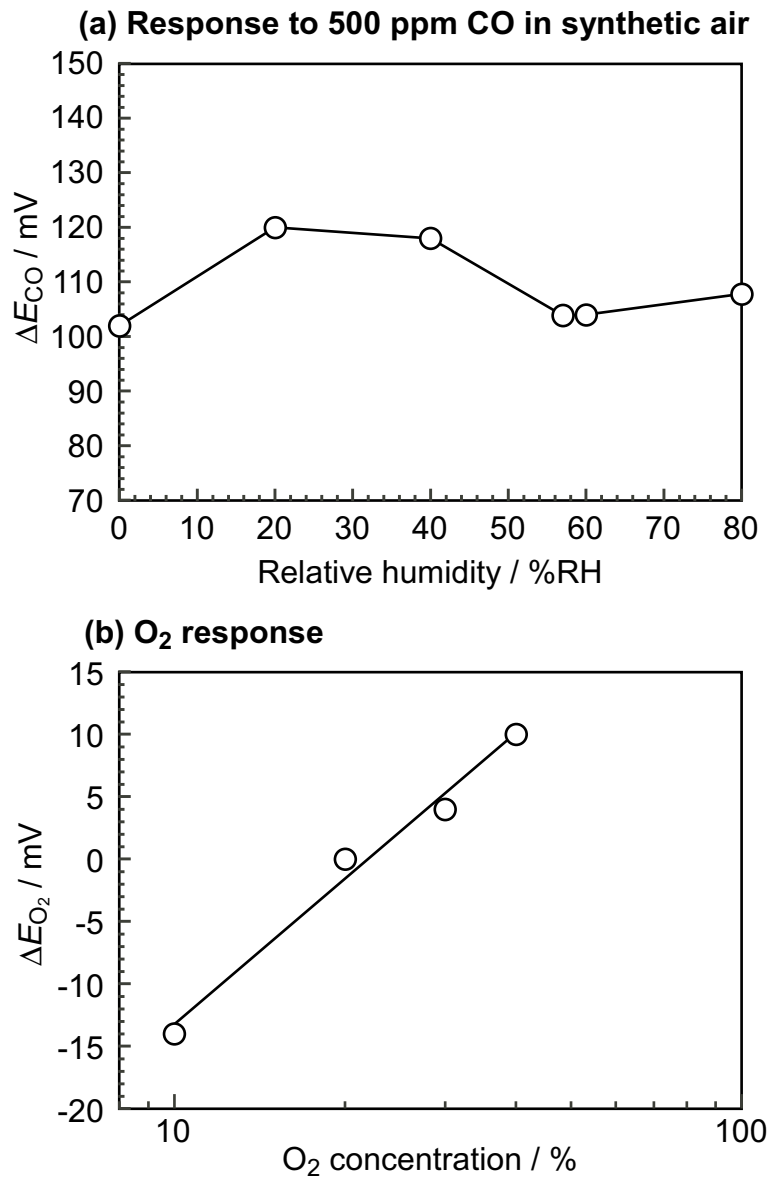


Fig. 5. Hyodo et al.

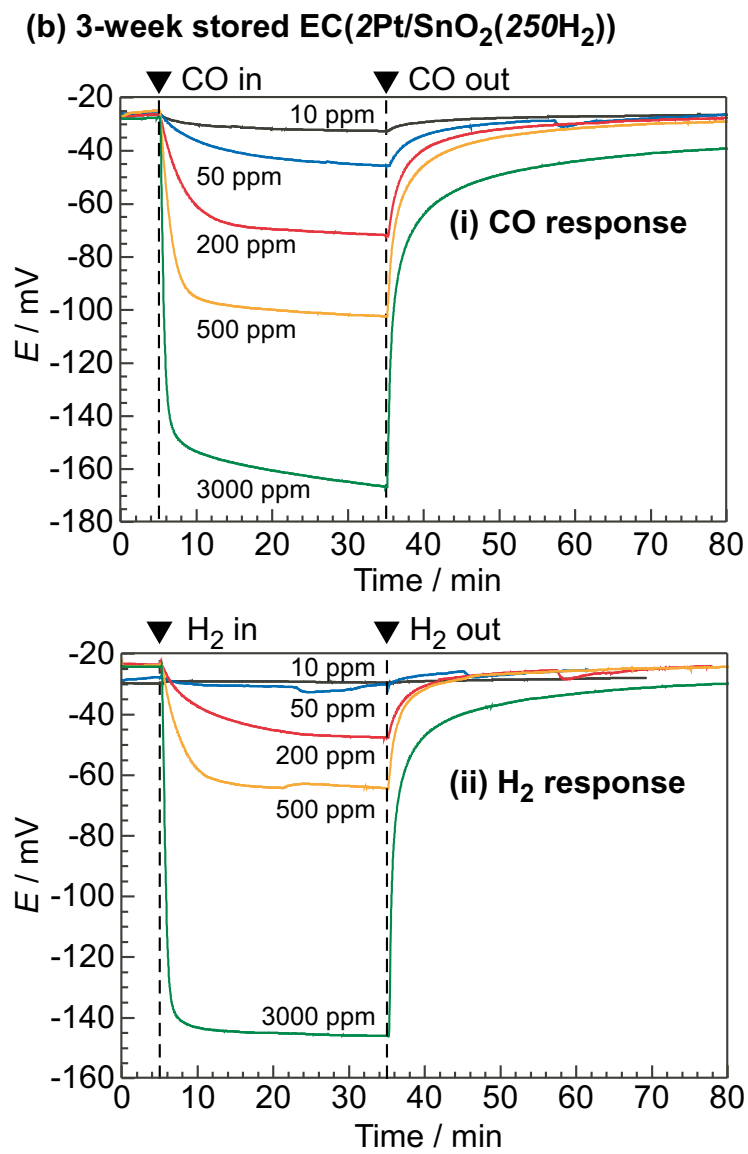
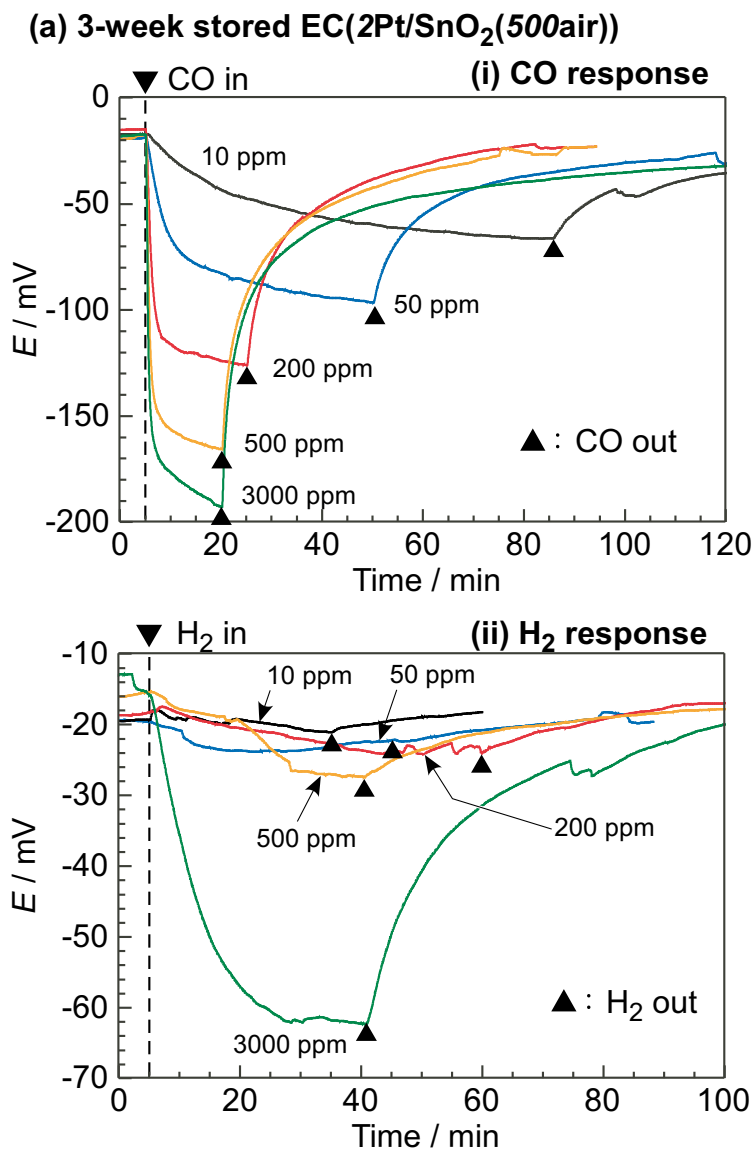


Fig. 6. Hyodo et al.

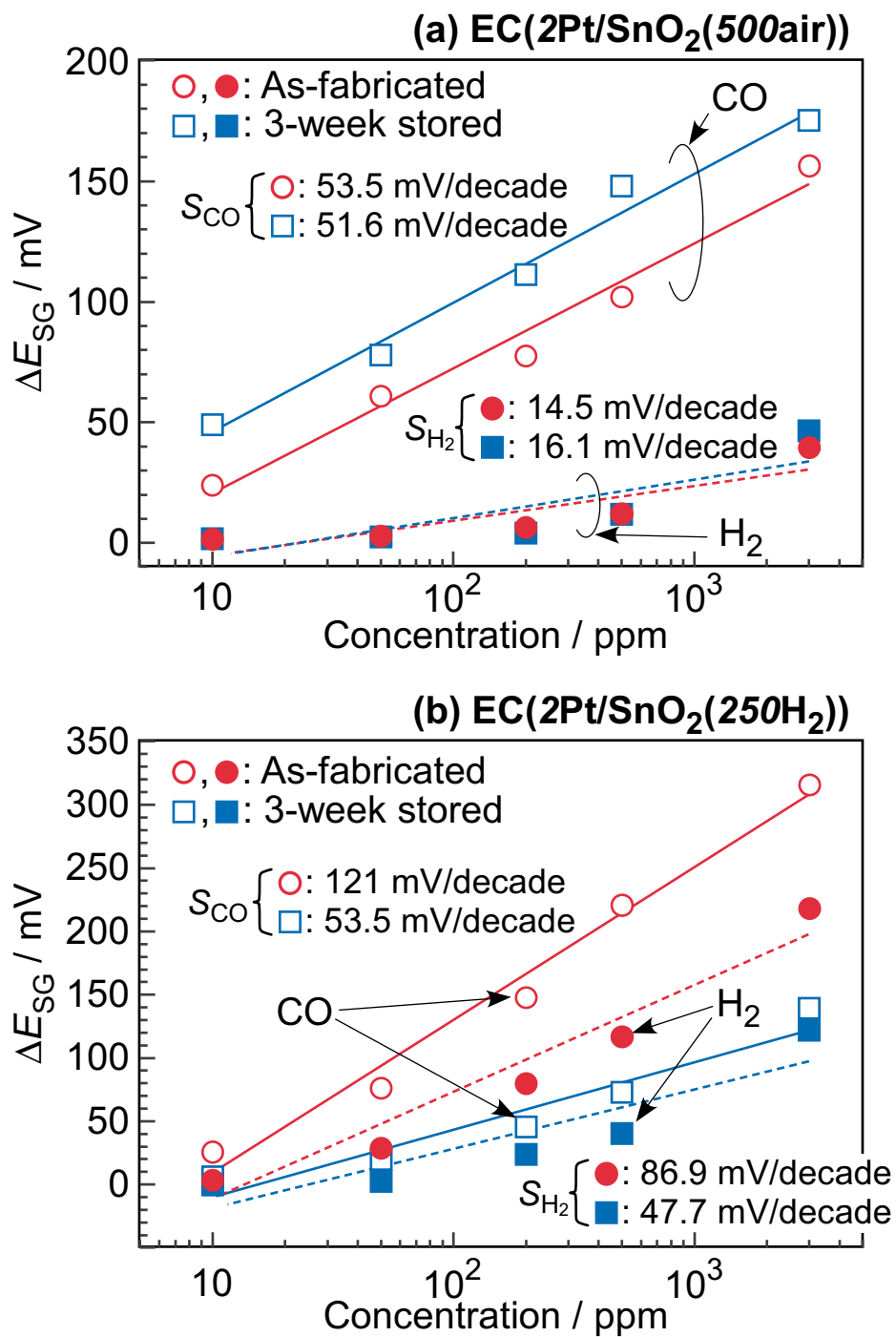


Fig. 7. Hyodo et al.

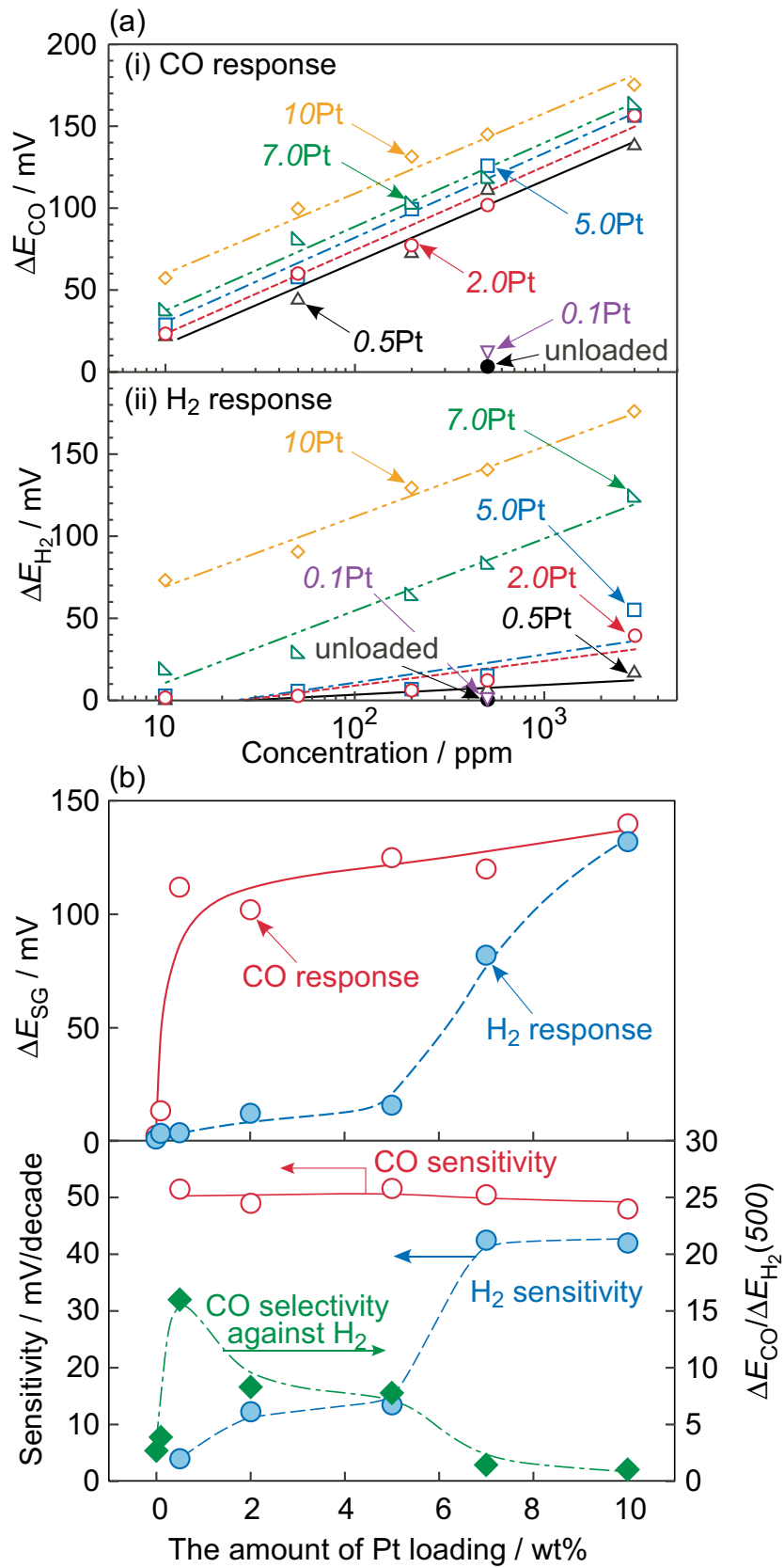


Fig. 8. Hyodo et al.

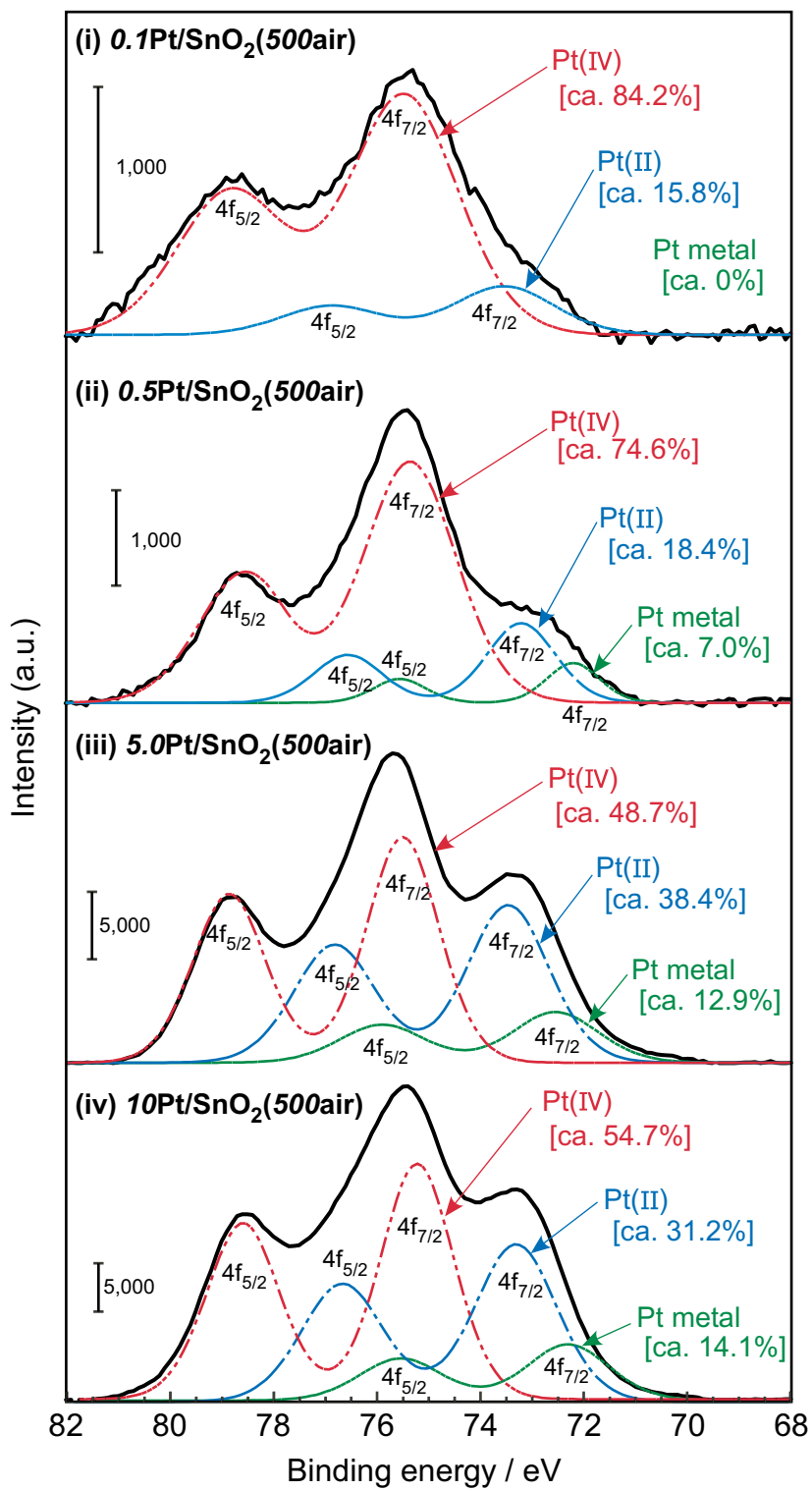


Fig. 9. Hyodo et al.

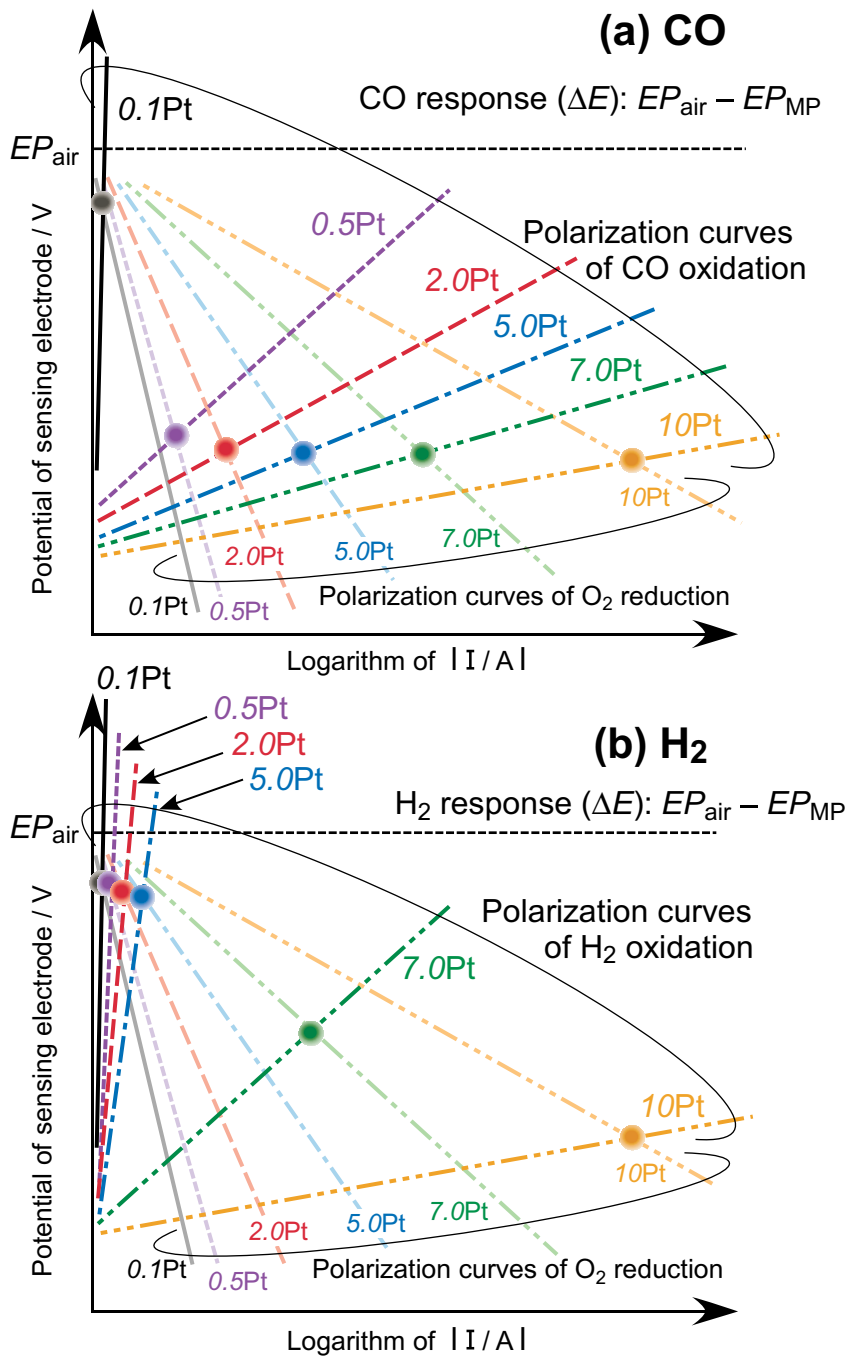


Fig. 10. Hyodo et al.

Supporting Information

Effects of Pt loading onto SnO₂ electrodes on CO-sensing properties and mechanism of potentiometric gas sensors utilizing an anion-conducting polymer electrolyte

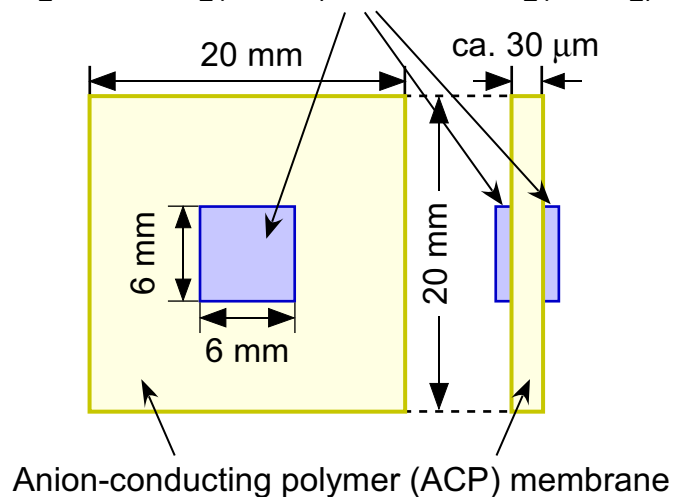
Takeo Hyodo*, Toshiyuki Goto, Mari Takamori, Taro Ueda, and Yasuhiro Shimizu

*Graduate School of Engineering, Nagasaki University
1-14 Bunkyo-machi, Nagasaki 852-8521, Japan*

*Corresponding author: hyodo@nagasaki-u.ac.jp

(a) Sensor element (electrochemical cell, EC)

SnO_2 , $n\text{Pt}/\text{SnO}_2(500\text{air})$, or $n\text{Pt}/\text{SnO}_2(250\text{H}_2)$ electrode



(b) Gas-sensing measurement system

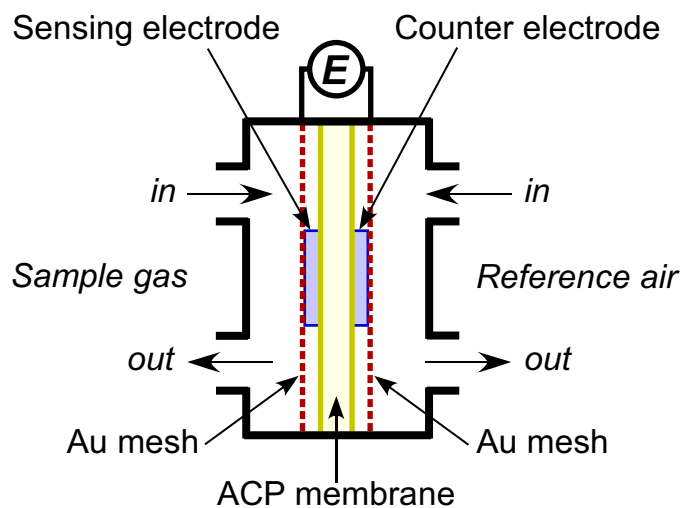


Figure S1. Schematic drawings of (a) sensor element and (b) gas-sensing measurement system with two electrode compartments.

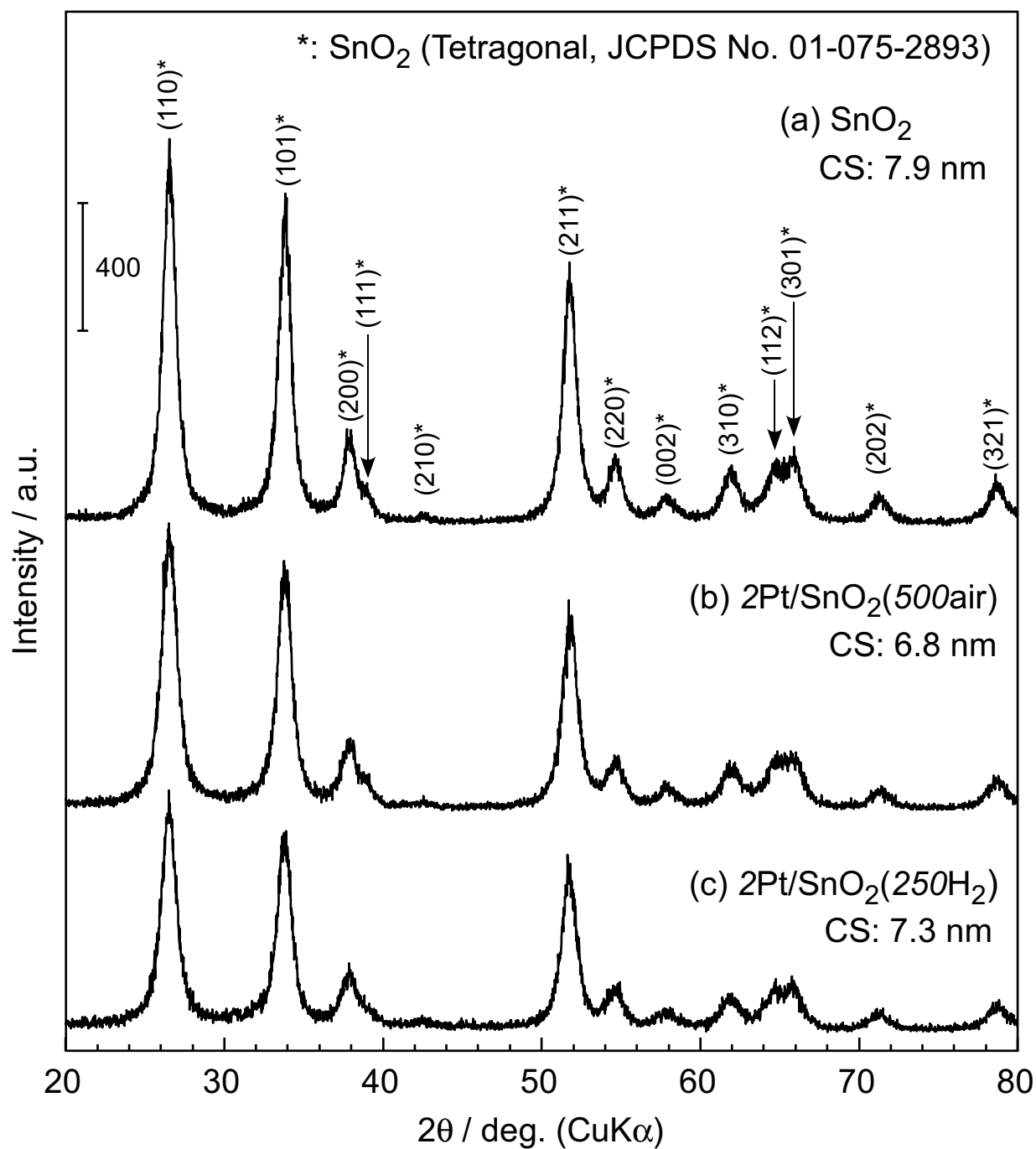


Figure S2. XRD spectra of pristine SnO₂, 2Pt/SnO₂(500air), and 2Pt/SnO₂(250H₂) powders, together with their crystallite size (CS).

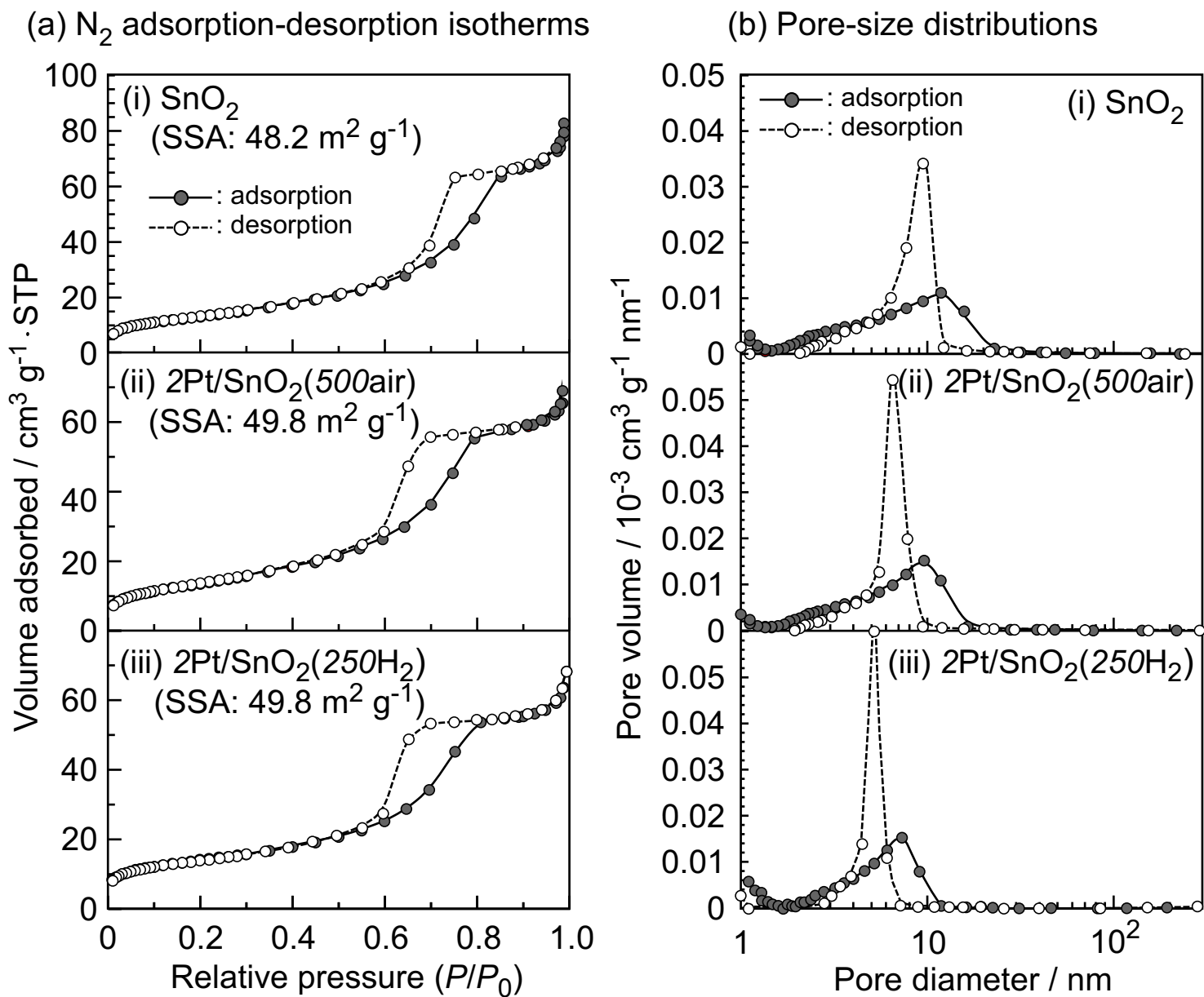


Figure S3. N_2 adsorption-desorption isotherms with specific surface area (SSA) and pore-size distributions of pristine SnO_2 , $2Pt/SnO_2(500air)$, and $2Pt/SnO_2(250H_2)$ powders.

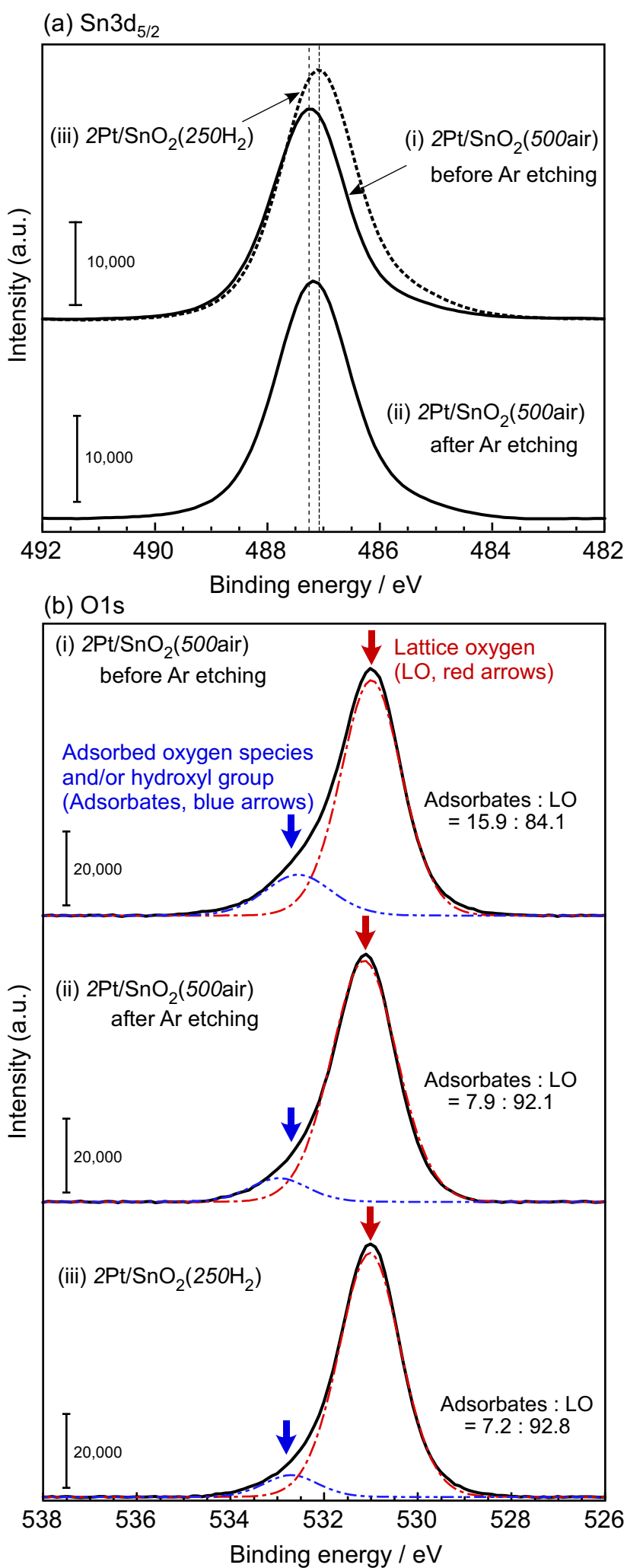


Figure S4. XPS spectra of Sn 3d_{5/2} and O 1s of 2Pt/SnO₂(500air) and 2Pt/SnO₂(250H₂) powders.

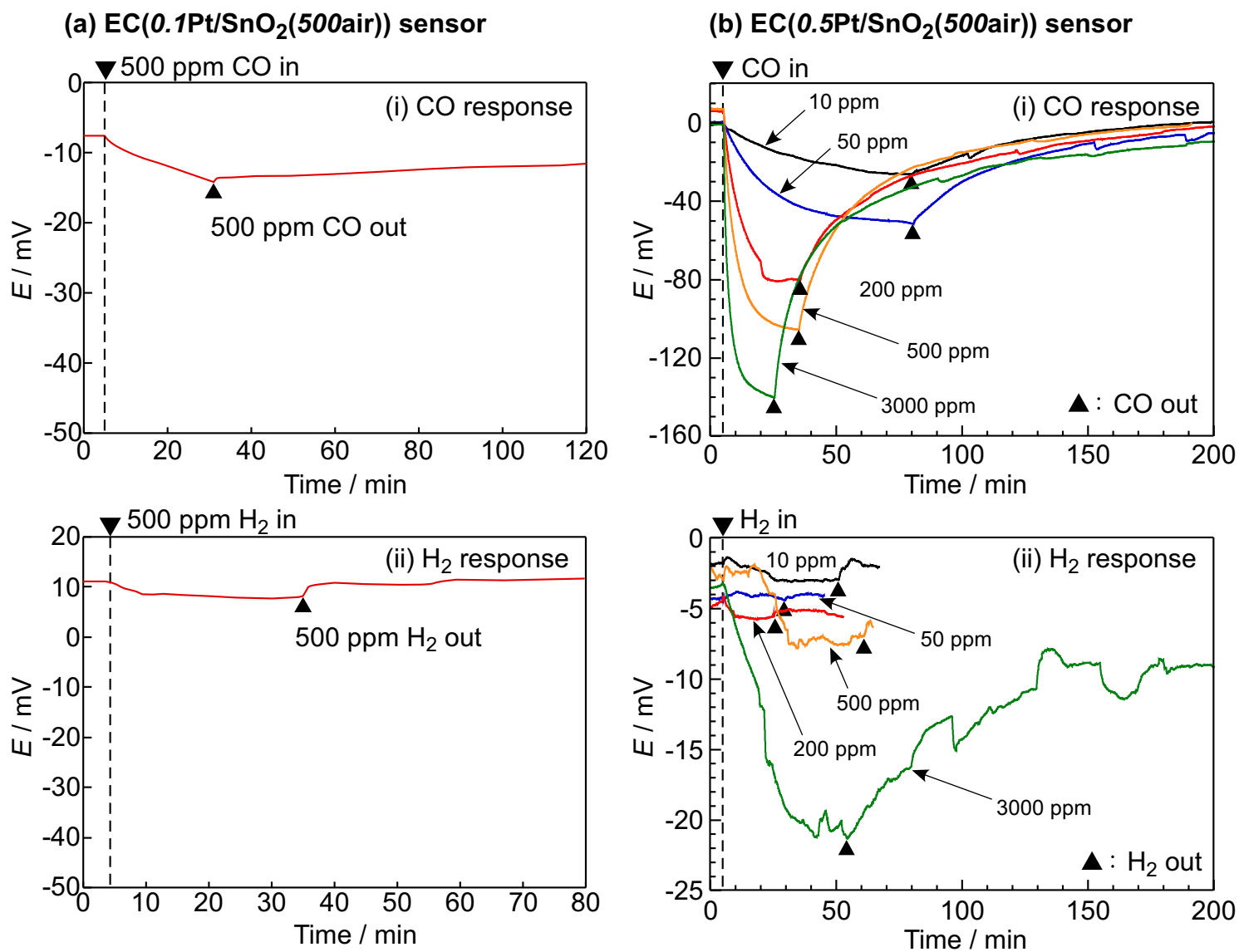


Figure S5. Response transients of EC(0.1Pt/SnO₂(500air)) and EC(0.5Pt/SnO₂(500air)) sensors to CO and H₂ in synthetic air 30°C (57%RH).

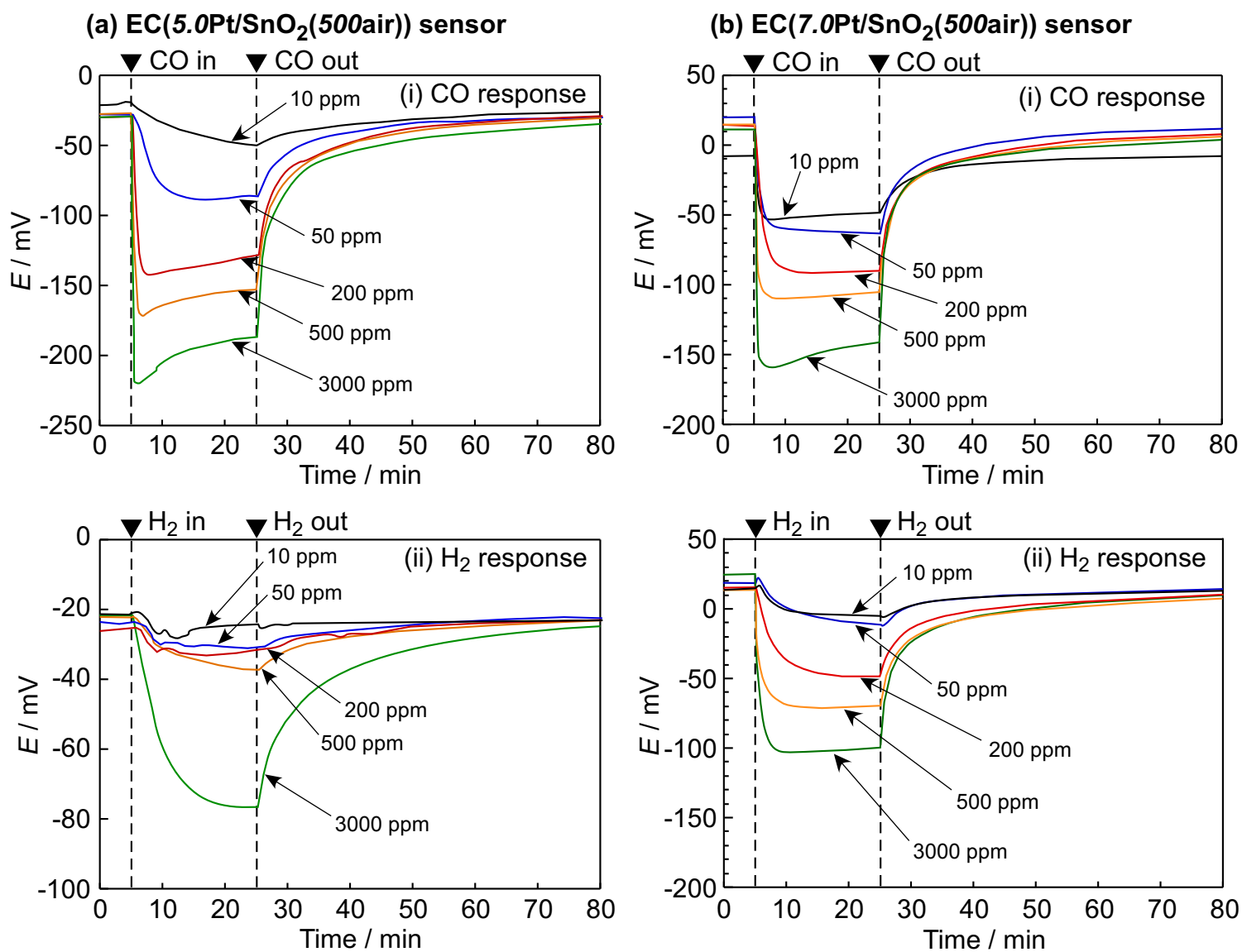


Figure S6. Response transients of EC(5.0Pt/SnO₂(500air)) and EC(7.0Pt/SnO₂(500air)) sensors to CO and H₂ in synthetic air 30°C (57%RH).

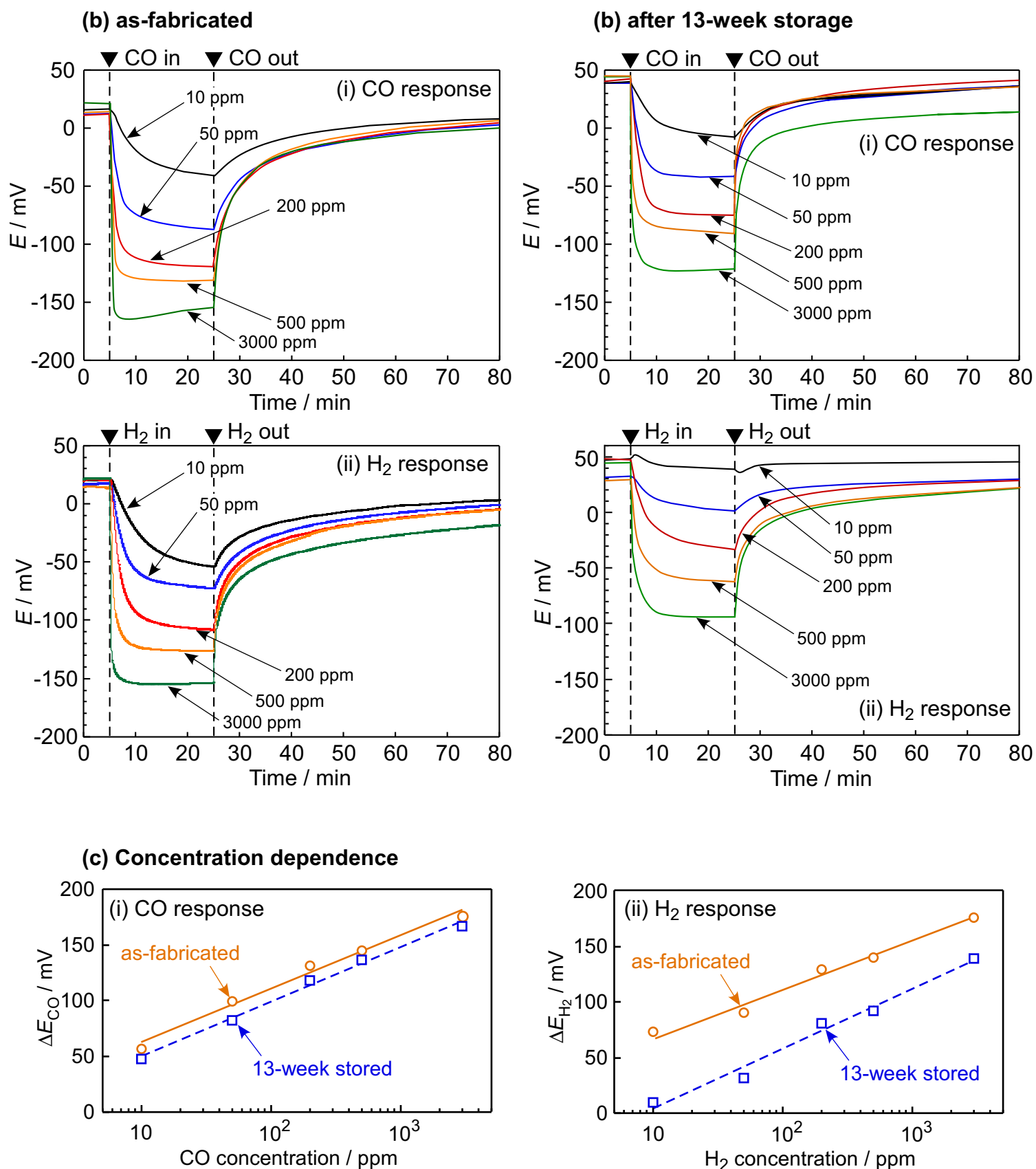


Figure S7. Response transients to CO and H₂ and concentration dependences on CO and H₂ responses of as-fabricated and 13-week stored EC(10Pt/SnO₂(500air)) sensor in synthetic air 30°C (57%RH).

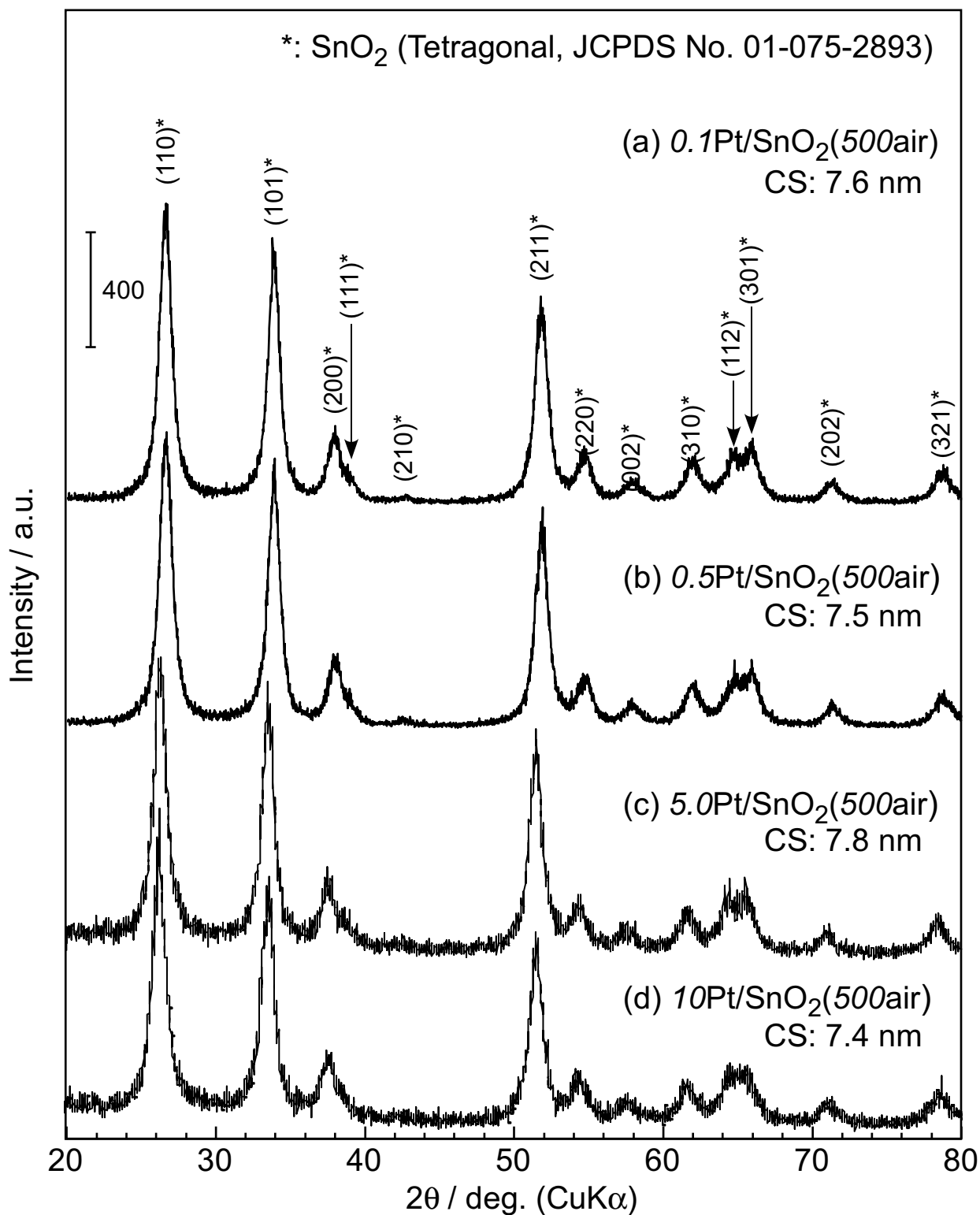


Figure S8. XRD spectra of typical n Pt/SnO₂(500air) powders, together with their crystallite size (CS).

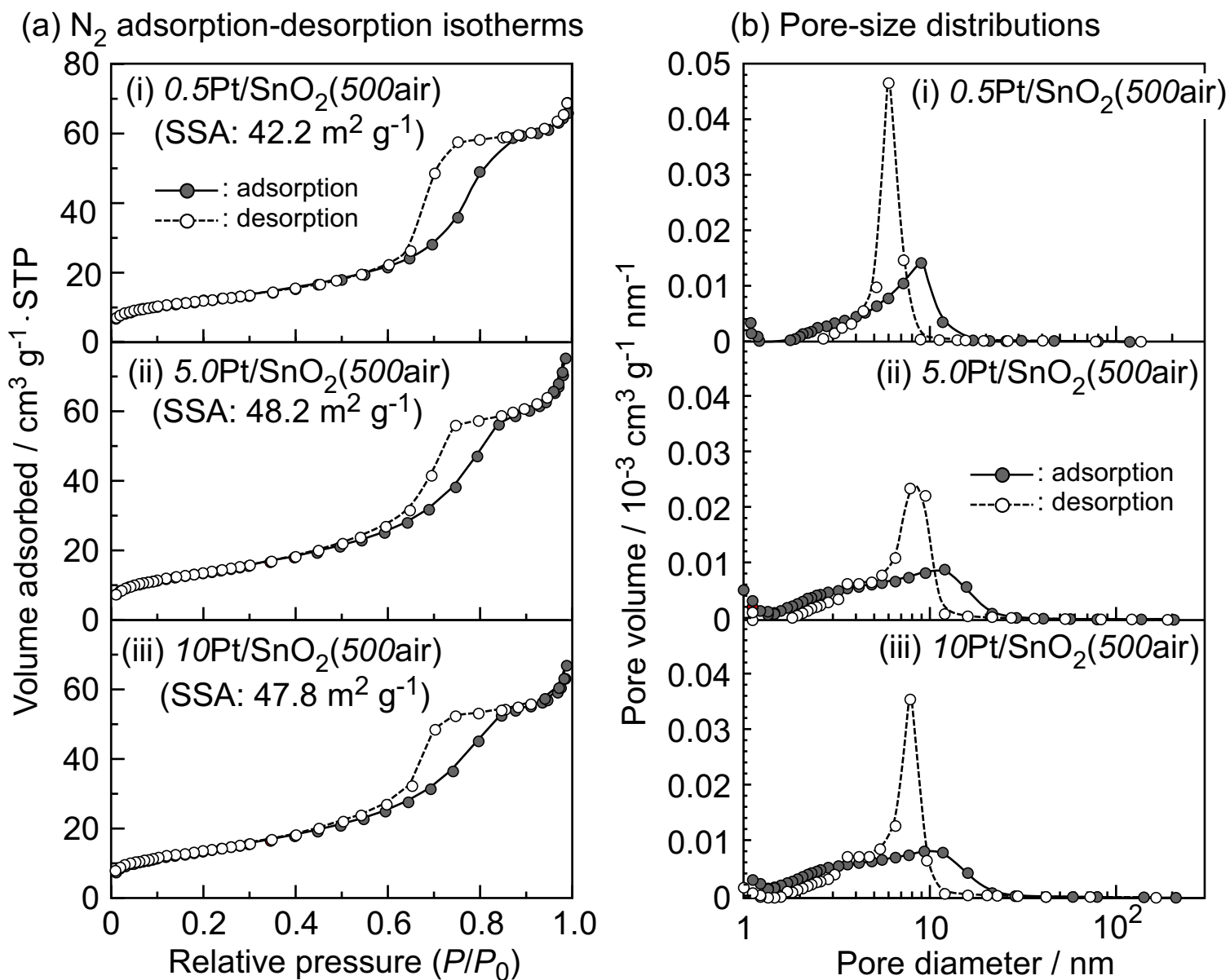


Figure S9. (a) N₂ adsorption-desorption isotherms with specific surface area (SSA) and (b) pore-size distributions of typical n Pt/SnO₂(500air) powders (n : 0.5, 5.0, 10).

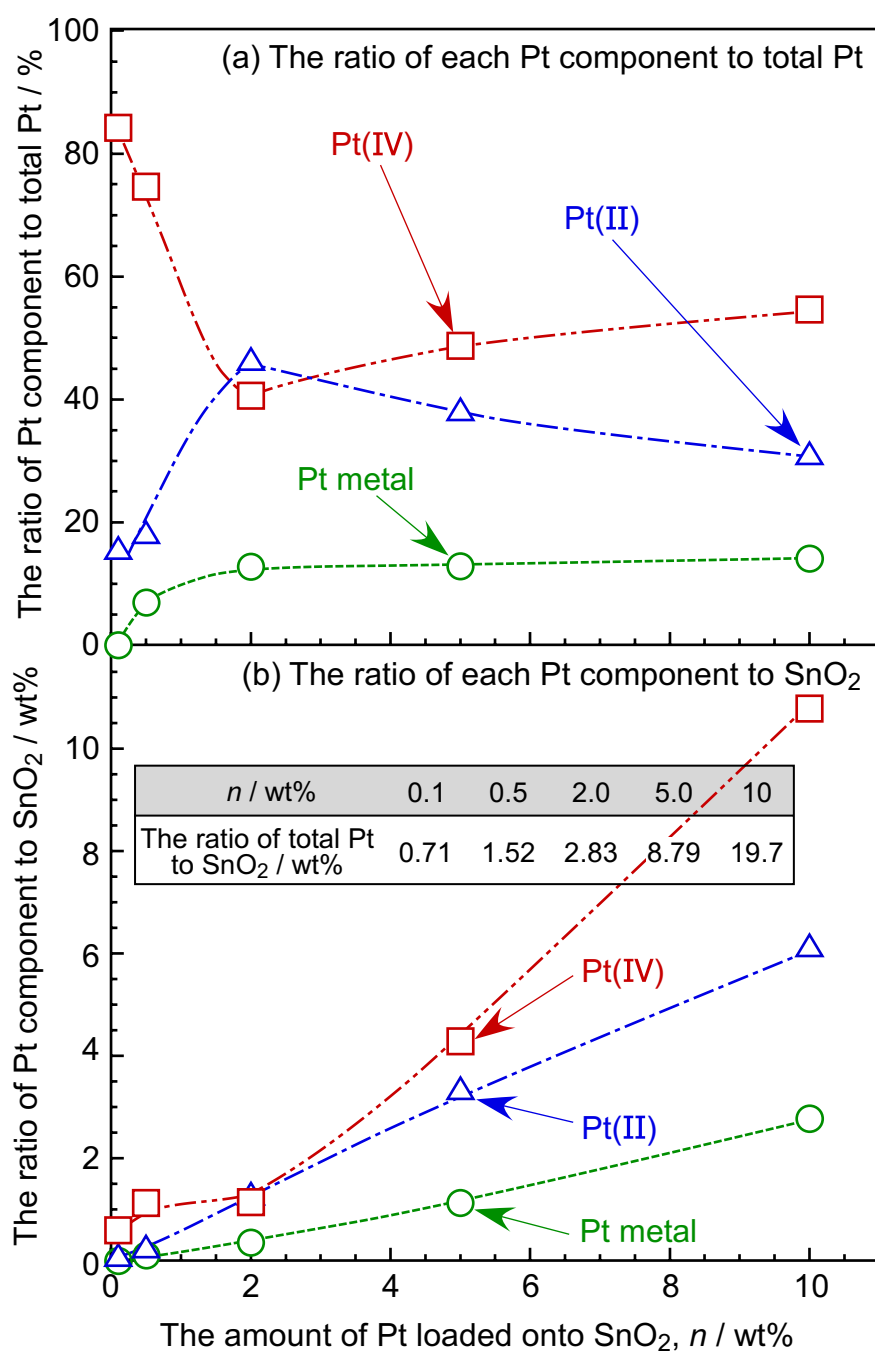


Figure S10. Variations in the ratio of each Pt component to total Pt and SnO₂ of typical $n\text{Pt}/\text{SnO}_2(500\text{air})$ powders with the amount of Pt loaded onto SnO₂, together with the ratio of total Pt to SnO₂. All the ratios were calculated by deconvolution of their Pt 4f XPS spectra.

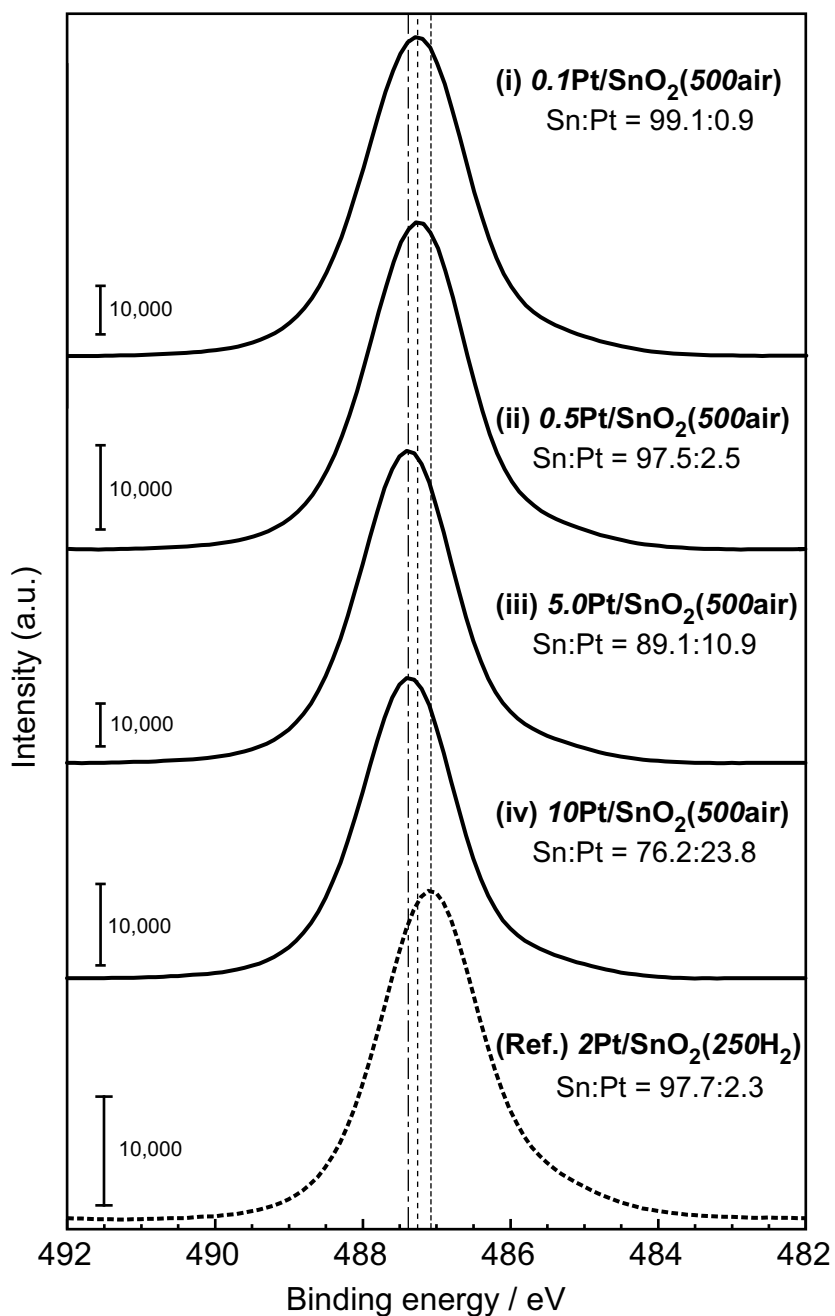


Figure S11. XPS spectra of Sn 3d_{5/2} of typical *n*Pt/SnO₂(500air) powders (*n*: 0.1, 0.5, 5.0, 10), together with that of 2Pt/SnO₂(250H₂) powder as a reference.

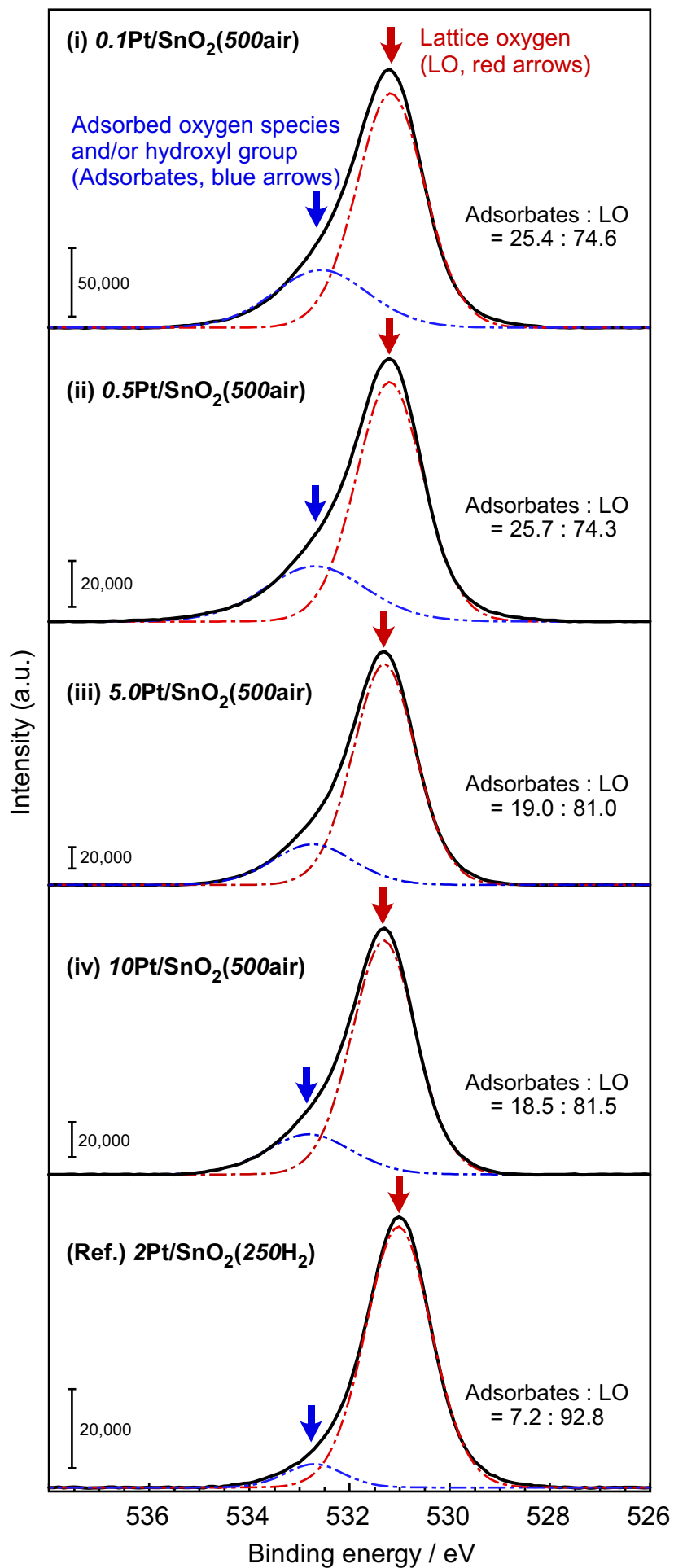
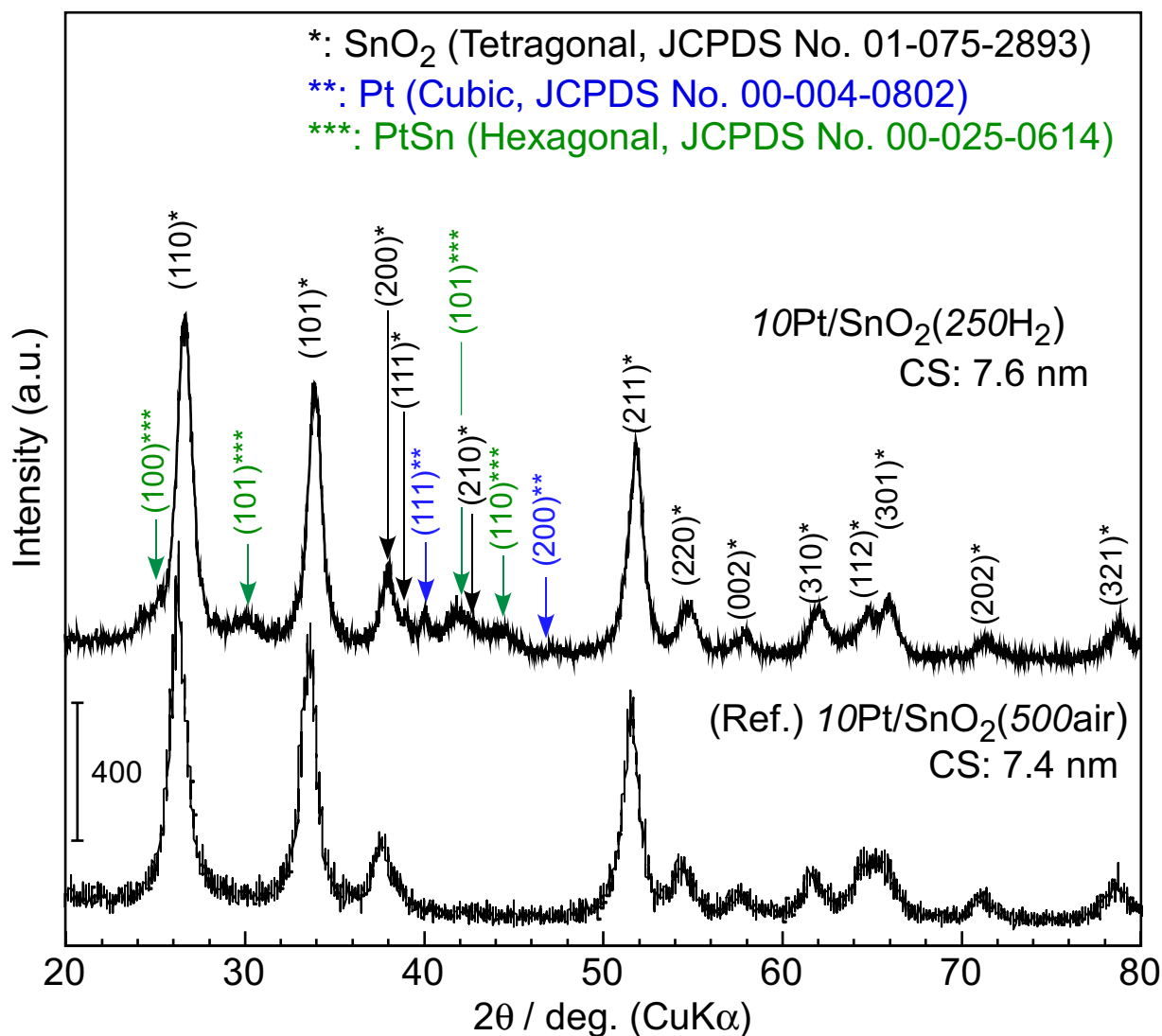
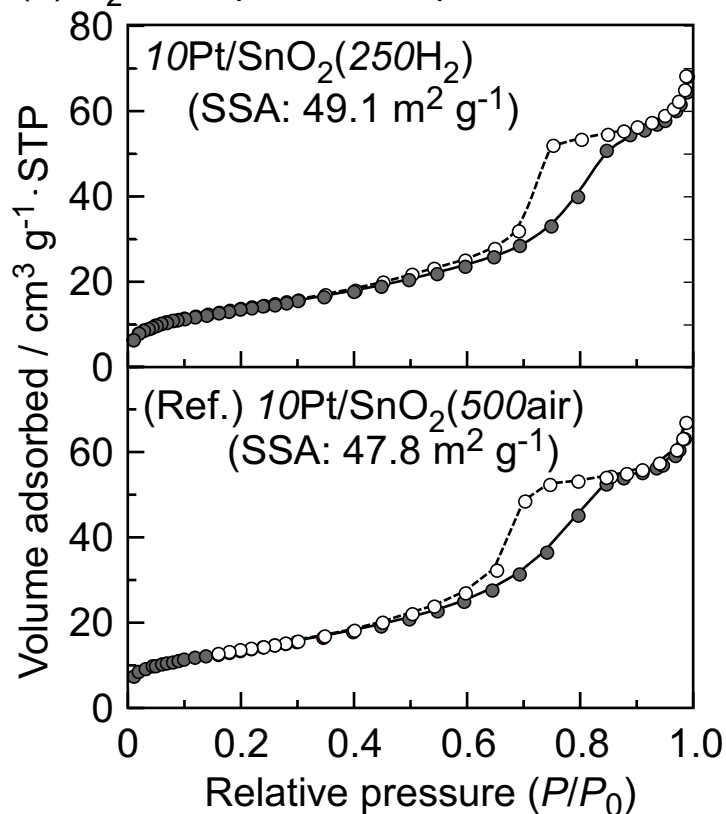


Figure S12. XPS spectra of O 1s of typical n Pt/SnO₂(500air) powders (n : 0.1, 0.5, 5.0, 10), together with that of 2Pt/SnO₂(250H₂) powder as a reference.

(a) XRD spectra



(b) N₂ adsorption-desorption isotherms



(c) Pore-size distributions

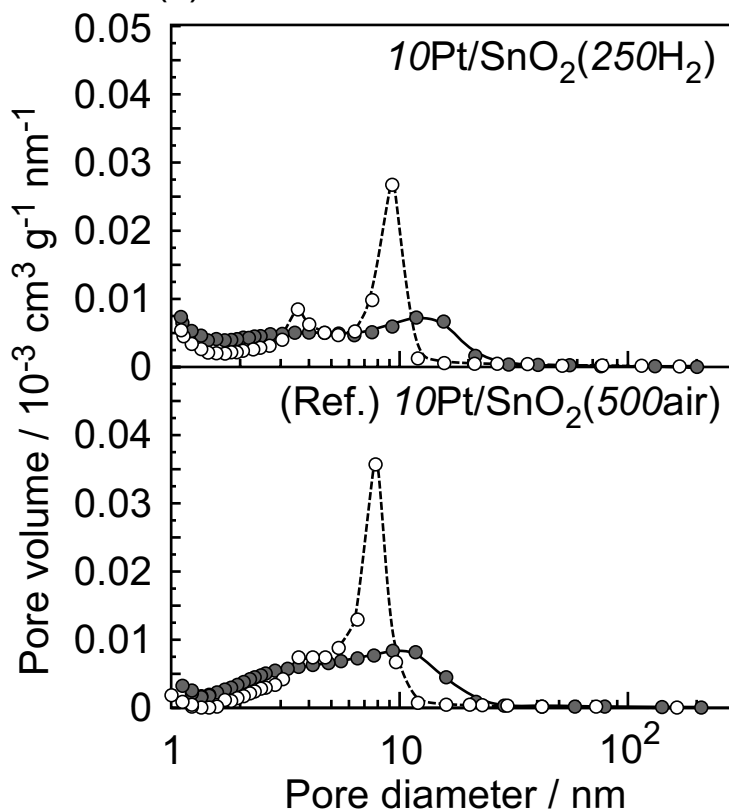


Figure S13. XRD spectrum, N₂ adsorption-desorption isotherms, and pore-size distributions of 10Pt/SnO₂(250H₂) powder, together with those of 10Pt/SnO₂(500air) powder as a reference.

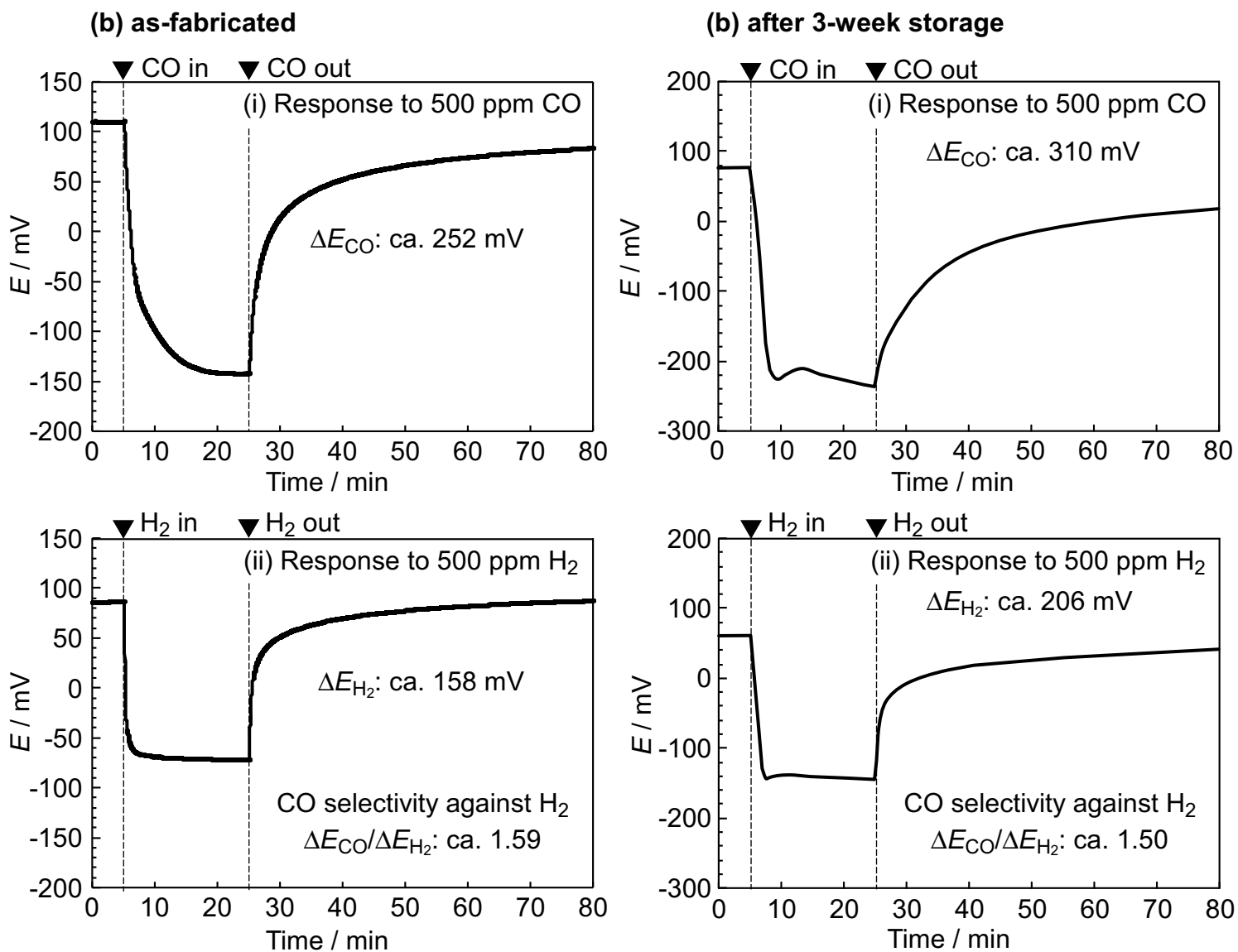


Figure S14. Response transients of as-fabricated and 3-week stored EC(10Pt/SnO₂(250H₂)) sensors to 500 ppm CO and H₂ in synthetic air 30°C (57%RH).

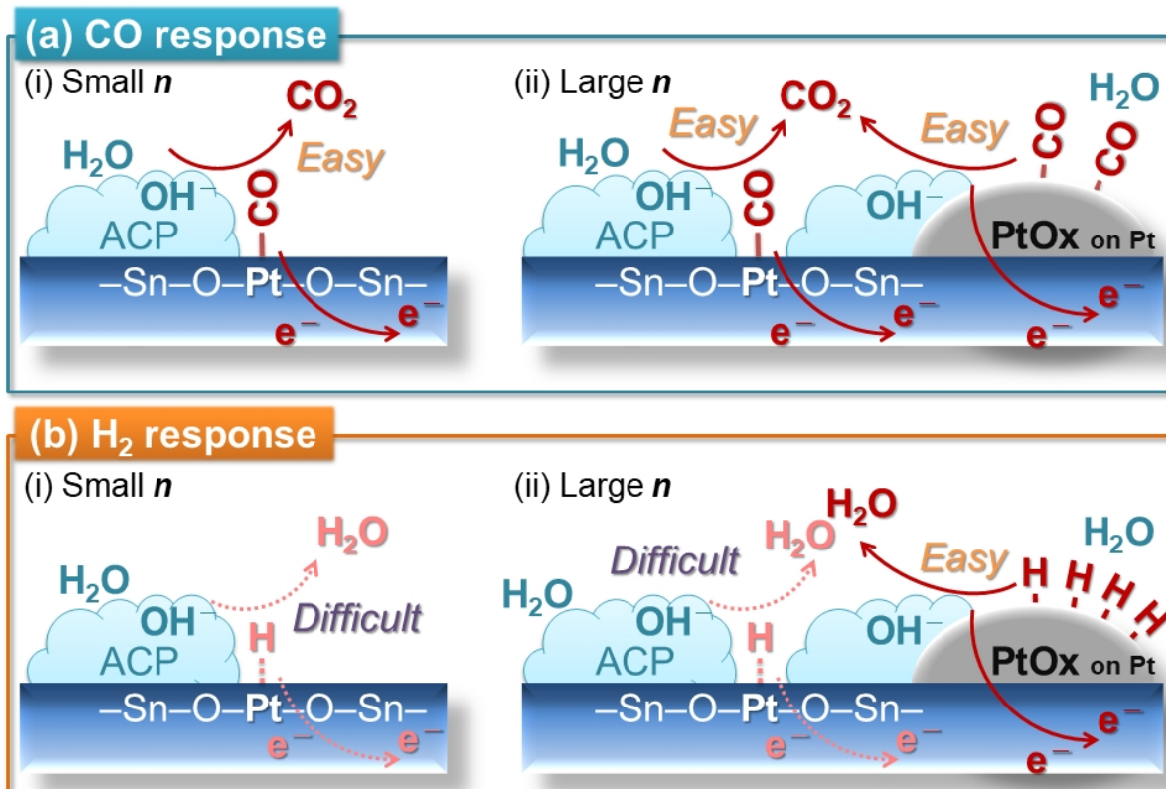


Figure S15. Possible process of CO and H₂ anodic reactions on $nPt/SnO_2(500air)$ electrode surface.